ISSN 0915-633X

NATIONAL INSTITUTE FOR FUSION SCIENCE

Adiabatic Invariant and Evaluation of Particle Loss in Helical Torus

J. Todoroki

(Received – Aug. 28, 1989)
(Revised – Jan. 16, 1990)

NIFS-10 Feb. 1990

RESEARCH REPORT
NIFS Series

NAGOYA, JAPAN

Adiabatic Invariant and Evaluation of Particle Loss in Helical Torus

Jiro TODOROKI

National Institute for Fusion Science, Nagoya, 464-01

(Received - Aug. 28, 1989)
(Revised - Jan. 16, 1990)

Abstract

Analytic expression for the longitudinal adiabatic invariant is derived for general magnetic configuration. The orbit loss is evaluated to determine the outermost loss-free surface. Geometrical factor of the neoclassical transport coefficients in $1/\nu$ regime in helical torus is calculated by using the longitudinal adiabatic invariant. The dependence of the particle confinement upon the geometrical parameter is investigated for N=10 configurations; and the improvement by the inward shift of the magnetic axis is quantitatively clarified.

KEYWORDS: adiabatic invariant, particle loss, helical torus, LHS, neoclassical transport, numerical calculation, stellarator

§1. Introduction

The knowledge of particle orbit is important to understand the plasma confinement in the toroidal helical devices. Usually the particle orbit is studied by integrating the drift equation of motion in the given magnetic field; such calculations are quite complicated and time-consuming one. The simple description with the use of longitudinal adiabatic invariant [1-6] is useful in many cases, and the transport theory in the rare collision case is based on such description. However, the analytic representation of the longitudinal adiabatic invariant $J_{/\!/}$ has been known only for simple model fields, which are not sufficient for actual magnetic configurations.

In this paper, the analytic representation for the longitudinal adiabatic invariant for the general magnetic configuration is presented, in the convenient form for the numerical calculations for actual magnetic field configurations. Such expression employs a powerful method to investigate the particle confinement in the wide range of parameter space specifying the magnetic field configurations.

Application to the evaluation of the particle loss and to the calculation of neoclassical transport coefficients in $1/\nu$ regime is also discussed. Especially, the effects of magnetic axis shift by vertical field, shaping of averaged surface by quadrupole field, and the pitch modulation of the helical coils are investigated. In the design study of Large-Scaled Helical System (LHS)[7,8] the confinement of single particles is one of the key issues to choose the magnetic configuration. It is found that in the low N devices the particle confinement as well as the MHD beta limit is improved by the inward shift of the plasma. As the

characteristic number signifying the performance of particle confinement of each configuration the radius of the such a magnetic surface that the particle starting within the surface never reach to the loss boundary (outermost loss-free surface) is employed. The application of the adiabatic invariant analysis to this problem recover the results obtained in the design study; and it allows us to extend easily to the wider range of parameters. The investigation is restricted to the vacuum magnetic field.

In the next section the longitudinal adiabatic invariant in the helical torus is introduced. The method to calculate the adiabatic invariant in the actual magnetic field is presented in §3. The method to determine the largest surface without orbit loss is described in §4. The particle transport in $1/\nu$ regime is discussed in §5. The application of the adiabatic invariant to these problems is given in §6, for the magnetic field configuration used in LHS design studies, mainly for N=10, γ_c=1.20 configurations, γ_c being the pitch parameter [see. eq.(6.3)]. Some examples for N=8 configurations are also discussed. The summary is given in the last section. Some formulae useful to calculate adiabatic invariant and the related integral are given in the Appendixes.

§2. Adiabatic Invariant

We use the magnetic coordinates (ψ, θ, φ), in which the magnetic field can be expressed as

$$B = \nabla\psi\times\nabla\theta - \nabla\Psi_p(\psi)\times\nabla\varphi = B_\varphi\nabla\varphi + B_\theta\nabla\theta + B_\psi\nabla\psi. \qquad (2.1)$$

Magnetic lines of force are straight in φ-θ plane with the rotational

transform $\iota(\psi) = d\Psi_p/d\psi$ in this coordinates. The choice of θ and φ has still one freedom. Usually they are chosen so that the covariant component B_θ and B_φ of the magnetic field are constant on the magnetic surfaces.[9] However we do not restrict ourselves to this special choice. In the helical torus with our interest, the system has many period $N \gg 1$ in toroidal direction, and the rotational transform per period is small, $\iota/N \ll 1$. Under these assumptions, the particle motion can be separated into the fast periodic motion in φ direction and the slower motion perpendicular to this direction. After averaging with respect to the fast periodic motion in φ direction, the slower motion in the poloidal cross section is described in terms of the longitudinal adiabatic invariant.

The longitudinal adiabatic invariant $J_{/\!/}$ is defined as

$$J_{/\!/} = J_T \equiv \oint \frac{m v_{/\!/} B_\varphi}{B} d\varphi, \tag{2.2a}$$

for ripple trapped particles, and

$$J_{/\!/} = J_\pm \equiv \int_0^{2\pi/N} \frac{m|v_{/\!/}|B_\varphi}{B} d\varphi \pm \frac{2\pi e}{N}\Psi_p(\psi), \tag{2.2b}$$

for passing particles.[5,6] Here the integration is carried out for ψ and θ fixed. The sign $\pm$ in eq.(2.2b) corresponds to the direction of the particle movement. The parallel velocity $v_{/\!/}$ is

$$v_{/\!/} = \pm\sqrt{(2/m)(W - \mu B - e\Phi_s)}.$$

Here W is the energy, μ is the magnetic moment, m and e are mass and charge of the particle, and Φ_s is the static electric potential.

The particle motion in the poloidal cross section is described by the equations

$$\frac{d\psi}{dt} = \frac{1}{e}\frac{\partial J_{/\!/}}{\partial\theta}\Big/\frac{\partial J_{/\!/}}{\partial W}, \qquad \frac{d\theta}{dt} = -\frac{1}{e}\frac{\partial J_{/\!/}}{\partial\psi}\Big/\frac{\partial J_{/\!/}}{\partial W}. \tag{2.3}$$

In these equations, the variables ψ and θ are not the coordinates of the real particles, but those of some kind of average with respect to the fast motion along φ direction. The actual position of the particles can be known when the phase of the fast motion is specified. The detail of such formulation will be given in the other paper.[6]

§3. Calculation of Adiabatic Invariant

In this section we consider the concrete expression for the adiabatic invariant. The electrostatic potential is assumed as the function of ψ and θ only.

The magnetic field can be expressed in terms of Fourier series

$$B(\psi,\theta,\varphi) = \sum_{m,n} B_{m,n}(\psi) \cos(m\theta - nN\varphi). \tag{3.1}$$

The symmetry $B(\psi,-\theta,-\varphi)=B(\psi,\theta,\varphi)$ is assumed, so that only cosine terms appear in this expression. If such symmetry does not exist, the sine terms appear in the expansion. This can also expressed in the form

$$B(\psi,\theta,\varphi) = B_0 \sum_{n=0}^{\infty} \varepsilon_n(\psi,\theta) \cos(nN\varphi - \delta_n(\psi,\theta)). \tag{3.2}$$

where ε_n and δ_n are defined by the relations,

$$B_0\varepsilon_n \cos\delta_n = \sum_m B_{m,n} \cos m\theta, \qquad B_0\varepsilon_n \sin\delta_n = \sum_m B_{m,n} \sin m\theta. \tag{3.3}$$

Here B_0 is the typical value of the magnetic field strength, which is introduced in order to make ε_n dimensionless. If the Fourier series in eq.(3.2) has only two coefficients $\varepsilon_0 \equiv \varepsilon_0$, and $\varepsilon_1 \equiv \varepsilon_1$, in the coordinate such that $B_\varphi \equiv R_0 B_0$, the adiabatic invariant eqs.(2.2) can be represented as

$$J_T = \frac{8R_0}{N}\left(\frac{m\mu B_0}{\varepsilon_H}\right)^{1/2} Q(C,\xi), \tag{3.4a}$$

$$J_\pm = \pm\frac{2\pi e}{N}\Psi_p + \frac{4R_0}{N}\left(\frac{m\mu B_0}{\varepsilon_H}\right)^{1/2} Q(C,\xi), \tag{3.4b}$$

where

$$\xi = \frac{\lambda-\varepsilon_T+\varepsilon_H}{2\varepsilon_H}, \quad C = \frac{\varepsilon_T-\varepsilon_H}{2\varepsilon_H}, \quad \lambda = \frac{W-e\Phi_E}{\mu B_0}. \tag{3.5}$$

The ripple trapped particles are characterized by $\xi<1$, and passing particles by $\xi>1$. The function Q is given by

$$Q(C,\xi) = \left(1+\frac{\xi}{C}\right)\Pi_1\left(\frac{\xi}{C};\xi\right) - K(\xi) \qquad \text{(for } \xi<1\text{)}, \tag{3.6a}$$

$$Q(C,\xi) = \frac{1}{\xi^{1/2}}\left\{\left(1+\frac{\xi}{C}\right)\Pi_1\left(\frac{1}{C};\frac{1}{\xi}\right) - K\left(\frac{1}{\xi}\right)\right\} \qquad \text{(for } \xi>1\text{)}, \tag{3.6b}$$

$$Q(C,1) = \frac{1}{C^{1/2}}\arctan\frac{1}{C^{1/2}}, \tag{3.6c}$$

where Π_1 is the complete elliptic integral of the third kind

$$\Pi_1(\nu;\xi) = \int_0^{\pi/2}\frac{d\varphi}{(1+\nu\sin^2\varphi)\sqrt{1-\xi\sin^2\varphi}}, \tag{3.7}$$

and K is the complete elliptic integral of the first kind.

In the case of multiple n, the situation is much more complicated in general. However, if the bump of the magnetic field is one in each period, in spite of many n modes, the adiabatic invariant can be expressed in terms of elliptic integrals. For this purpose let us introduce new angle variable $\chi(\psi,\theta,\varphi)$, such that the magnetic field strength can be expressed in the form:

$$B(\psi,\theta,\varphi) = B_0\{\varepsilon_T(\psi,\theta)+\varepsilon_t(\psi,\theta)\cos N\chi\}, \tag{3.8}$$

or

$$\varepsilon_t = \frac{B_{max}+B_{min}}{2B_0}, \quad \varepsilon_h = \frac{B_{max}-B_{min}}{2B_0}, \quad \chi = \frac{1}{N}\arccos\left(\frac{B-B_0\varepsilon_t}{B_0\varepsilon_h}\right), \tag{3.9}$$

where $B_{max}(\psi,\theta)$ and $B_{min}(\psi,\theta)$ are the maximum and minimum of the magnetic field strength with respect to φ; and let us assume the Fourier expansion

$$\frac{B_\varphi}{R_0B_0}\frac{d\varphi}{d\chi} = 1+\sum_{n=1}^{\infty}\{a_n(\psi,\theta)\cos(nN\chi)+b_n(\psi,\theta)\sin(nN\chi)\}. \tag{3.10}$$

The Fourier coefficients are calculated simply as

$$a_n = \frac{N}{\pi R_0B_0}\int_0^{2\pi/N} B_\varphi\cos(nN\chi)d\varphi, \quad b_n = \frac{N}{\pi R_0B_0}\int_0^{2\pi/N} B_\varphi\sin(nN\chi)d\varphi. \tag{3.11}$$

We shall consider the following integral

$$I(C,\xi) = \int_0^{\frac{\pi}{2}}\frac{\xi\cos^2\theta}{(C+\xi\sin^2\theta)\sqrt{1-\xi\sin^2\theta}} \times\left\{1+\sum_{n=0}^{\infty}(-1)^n a_nT_n(1-2\xi\sin^2\theta)\right\}d\theta, \tag{3.12a}$$

for the case of $\xi\leqq 1$, and

$$I(C,\xi) = \int_0^{\frac{\pi}{2}}\frac{\sqrt{\xi-\sin^2\theta}}{C+\sin^2\theta}\left\{1+\sum_{n=0}^{\infty}(-1)^n a_nT_n(1-2\sin^2\theta)\right\}d\theta, \tag{3.12b}$$

for the case of $\xi>1$. Here, $T_n(x)=\cos(n\arccos x)$ is the Chebyshev polynomials of the first kind. The coefficients b_n do not appear in the expression, because terms containing them are odd functions. Then we can write eqs.(2.2) in the form

$$J_r = \frac{8R_0}{N}\left(\frac{m\mu B_0}{\varepsilon_h}\right)^{1/2} I(C,\xi), \tag{3.13a}$$

$$J_\pm = \pm\frac{2\pi e}{N}\Psi_p+\frac{4R_0}{N}\left(\frac{m\mu B_0}{\varepsilon_t}\right)^{1/2} I(C,\xi). \tag{3.13b}$$

We expand

$$T_n(1-2z) = T_n(1+2C)+(C+z)\sum_{m=0}^{n-1} g_{n,m}(C)z^m. \tag{3.14}$$

The coefficients in this expansion can be calculated by using the recurrence relations:

$$g_{n+1,m} = \begin{cases} 2g_{n,m}-4g_{n,m-1}-g_{n-1,m} & (\text{for } m\geqq 1), \\ 2g_{n,0}-g_{n-1,0}-4T_n(1+2C) & (\text{for } m=0), \end{cases} \tag{3.15}$$

with $g_{n,m}=0$ for $m\geqq n$, and

$$g_{1,0} = -2, \quad g_{2,1} = 8, \quad g_{2,0} = -8(C+1). \tag{3.16}$$

Further we introduce the integrals:

$$H_k(\xi) = \int_0^{\frac{\pi}{2}} \frac{\xi^{k-1}\cos^2\theta \sin^{2k}\theta}{\sqrt{1-\xi\sin^2\theta}}d\theta \quad (\text{for } \xi\leqq 1), \tag{3.17a}$$

$$H_k(\xi) = \int_0^{\frac{\pi}{2}} \sqrt{\xi-\sin^2\theta}\,\sin^{2k}\theta d\theta \quad (\text{for } \xi\geqq 1). \tag{3.17b}$$

Note that $H_k(1)=1/(2k+1)$, and $H_k(0)=0$. These functions can be also calculated by using the recurrence relations:

$$H_{k+1}(\xi) = \frac{1}{2k+3}\{2(k+1+k\xi)H_k(\xi)-(2k-1)\xi H_{k-1}(\xi)\}, \tag{3.18}$$

with

$$H_0(\xi) = E(\xi)-(1-\xi)K(\xi), \quad H_1(\xi) = \frac{1}{3}\{(2-\xi)E(\xi)-2(1-\xi)K(\xi)\}, \tag{3.19a}$$

for $\xi\leqq 1$, and

$$H_0(\xi)=\xi^{1/2}E(\xi^{-1}), \quad H_1(\xi)=\frac{\xi^{1/2}}{3}\{(2-\xi)E(\xi^{-1})-(1-\xi)K(\xi^{-1})\}, \tag{3.19b}$$

for $\xi\geqq 1$. Here E is the complete elliptic integral of the second kind. Then we can write eqs.(3.12) in the form

$$I(C,\xi) = \left\{1+\sum_{n=1}^{\infty}(-1)^n a_n T_n(1-2C)\right\}Q(C;\xi)+\sum_{n=1}^{\infty}\sum_{k=0}^{n-1}(-1)^n a_n g_{n,k}(C)H_k(\xi). \tag{3.20}$$

In the actual situation we can replace the infinite sum in eq.(3.20) by

the sum of the first couples of terms. The number of terms, of course, depends on the problem; usually the inclusion of α_1 or α_2 yields significant effects, but the effects of α_3 and α_4 are very small.

§4. Evaluation of Orbit Loss

The conventional method to evaluate the particle loss in the given magnetic field is to determine the velocity space loss region for specified points. The importance of loss region in real coordinate is realized, and the loss region in two dimension, major radius and pitch angle, for fixed energy of particle is introduced. Such figures are useful to understand a certain aspect of the confinement properties, but not so useful in comparison of a lot of field configurations. In the course of the LHS design study the radius of the largest magnetic surface such that the particle started from the surface never reach to the particle loss boundary (outermost loss-free surface) is employed as the characteristics signifying the quality of particle confinement of the magnetic configurations.[10] Such surface depends on the choice of the loss boundary as well as the electric potential and the energy of particles. The outermost magnetic surface is chosen as the loss boundary ψ_b, because the particle going out to the plasma surface suffers the charge exchange interaction with the ambient neutral particles. If we want to determine the outermost loss-free surface by directly integrating the drift equations of motion, the large amount of calculations for the various initial conditions uniformly distributed on the three dimensional space, pitch angle, poloidal and toroidal angles. The use of adiabatic

invariant drastically reduces necessary amount of computations.

The confinement of particles moving freely around the torus (transit particles) is generally good. Therefore the confinement of the trapped particle is our main concern. In the following analysis, the orbit of the passing particles are considered to follow the magnetic surface, *i.e.* $J_{\pm} \simeq \pm e\Psi_p$, for the sake of simplicity. We also assume the up-down symmetry for $\varepsilon_T, \varepsilon_H$, etc., and Φ_E, *i.e.*

$$\varepsilon_T(\psi,-\theta) = \varepsilon_T(\psi,\theta), \quad \varepsilon_H(\psi,-\theta) = \varepsilon_H(\psi,\theta), \text{ etc.},$$
$$\Phi_E(\psi,-\theta) = \Phi_E(\psi,\theta), \tag{4.1}$$

which follows from the symmetry given in eq.(3.1), in order to assure the closing of the particle orbit.

The loss-free surface can be determined by the following two mechanisms: the orbit of $v_{/\!/}=0$ particles and the orbit of the transition particles. We denote the loss-free surface determined by the former particles as ψ_{L0}, and by the latter particles as ψ_{Lt}. The outermost loss-free surface ψ_L is determined by the smaller one of ψ_{L0} and ψ_{Lt}.

The orbit of $v_{/\!/}=0$ particles are characterized by $\xi=0$, or $(W-e\Phi_E)/\mu=B_{min}$. If B_{min} on the magnetic axis satisfies the inequality

$$\max_{\theta} \left\{ B_{min}(\psi_b,\theta) / \left[1-\frac{e\Phi_E(\psi_b,\theta)}{W}\right] \right\} \geq B_{min}(0) / \left[1-\frac{e\Phi_E(0)}{W}\right], \tag{4.2}$$

the particles started from magnetic axis with $v_{/\!/}=0$ can reach to the loss boundary; therefore $\psi_{L0}=0$. If the above inequality does not hold, then the outermost loss-free surface ψ_{L0} for $v_{/\!/}=0$ particles is determined by the equation

$$\max_{\theta} \left\{ \frac{B_{min}(\psi_b,\theta)}{1-\frac{e\Phi_E(\psi_b,\theta)}{W}} \right\} = \min_{\theta} \left\{ \frac{B_{min}(\psi_{L0},\theta)}{1-\frac{e\Phi_E(\psi_{L0},\theta)}{W}} \right\}. \tag{4.3}$$

The other limit is determines by the blocked particles, making

transition from passing to ripple trapped state. On the given surface $\psi=\psi_t$, we will take a transition point (ψ_t,θ_t). The particles with the pitch angle $\lambda_{t0} \equiv W/\mu = B_{max}(\psi_t,\theta_t)\{1-e\Phi_E(\psi_t,\theta_t)/W\}^{-1}$, makes transition to the ripple trapped state on this point, leaving this point with the value of adiabatic invariant $J_t = J_r(\psi_t,\theta_t,\lambda_{t0})$. This value is compared with the value of J_r on the loss boundary. If the inequalities

$$\max_{\theta} J_r(\psi_b,\theta,\lambda_{t0}) \geq J_t \geq \min_{\theta} J_r(\psi_b,\theta,\lambda_{t0}), \tag{4.4}$$

hold for some value of θ_t, the particles making transition at that point can reach to the loss boundary; *i.e.* $\psi_{Lt} < \psi_t$. On the contrary, if the inequalities (4.4) do not hold for all values of θ_t, the particles making transition on the surface do not reach to the loss boundary; *i.e.* $\psi_{Lt} > \psi_t$. Thus we can determine ψ_{Lt} by simple iteration procedure.

If the electric field is large and its spatial structure is not simple, the points with same values of invariant may not necessarily be connected by the single orbit. In that case the more complete procedure to follow the orbit is required to determine the loss region.

§5. Neoclassical Transport Coefficient in $1/\nu$ regime

The neoclassical transport in $1/\nu$ regime is described by the bounce averaged kinetic equation

$$\dot{\psi}\frac{\partial f}{\partial \psi}+\dot{\theta}\frac{\partial f}{\partial \theta} = \langle \mathcal{C}(f) \rangle, \tag{5.1}$$

where $\langle \mathcal{C} \rangle$ is the bounce averaged collision operator. Assuming that $\nu \sim \dot{\theta} \gg \dot{\psi}/\Delta\psi$, where $\Delta\psi$ is the typical scale length in ψ direction, the lowest order distribution function becomes the local Maxwellian depending

on ψ. To the next order, neglecting the term $\dot{\theta}(\partial f_1/\partial\theta)$, we have[4]

$$\frac{1}{e}\frac{\partial J_{/\!/}}{\partial\theta}\frac{\partial f_0}{\partial\psi} = \nu\frac{\partial}{\partial\mu}\left(\mu M\frac{\partial f_1}{\partial\mu}\right), \tag{5.2}$$

with

$$M \equiv \oint\frac{mv_{/\!/}B_\varphi}{B^2}\mathrm{d}\varphi. \tag{5.3}$$

In writing these equations, we have employed the Lorentz collision operator. We also used the expression for $\dot{\psi}$ in terms of adiabatic invariant. The quantity M can be calculated in the similar way to $J_{/\!/}$, as is given in Appendix B. The contribution to the radial flux comes only from ripple trapped particles, and the particle flux Γ^ψ becomes to

$$V'\Gamma^\psi = -\frac{N}{2\pi e^2m^2}\oint\mathrm{d}\theta\int_0^\infty\frac{\mathrm{d}W}{\nu}\frac{\partial f_0}{\partial\psi}\int_0^{W/B_{\min}}\frac{\mathrm{d}\mu}{\mu M}\left|\int_\mu^{W/B_{\min}}\frac{\partial J_r}{\partial\theta}\mathrm{d}\mu'\right|^2, \tag{5.4}$$

V' being the specific volume. Here the electrostatic potential is assumed as $\Phi_e(\psi)$, and W is put in the place of $W-e\Phi_e$. The adiabatic invariant depends on θ through ξ as well as C and α_n. If we put $J_r=(8R_0/N)\sqrt{m\mu B_0}\,I_*(\xi,\theta)$, or $I_*\equiv I/\varepsilon_t^{1/2}$, and $M=(4R_0/N)\sqrt{m\mu/B_0}\,I_{**}(\xi,\theta)$, and change the variable of integration from μ to ξ, we obtain the expression

$$V'\Gamma^\psi = -\frac{8R_0}{e^2B_0}\frac{N}{m^{3/2}}\,S^{\mathrm{geo}}\int_0^\infty W^{5/2}\frac{1}{\nu}\frac{\partial f_0}{\partial\psi}\mathrm{d}W, \tag{5.5}$$

where S^{geo} is the geometrical factor

$$S^{\mathrm{geo}} \equiv \int_0^{2\pi}\frac{\mathrm{d}\theta}{2\pi}(2\varepsilon_a)^{1/2}\int_0^1\frac{\mathrm{d}\xi}{(C+\xi)^{1/2}}\frac{1}{I_{**}(\xi,\theta)}$$

$$\times\left|I_*(\xi,\theta)\frac{2}{3}\frac{\partial}{\partial\theta}\{2\varepsilon_a(C+\xi)\}^{-3/2}+\frac{\partial}{\partial\theta}\int_0^\xi\frac{I_*(\xi',\theta)\mathrm{d}\xi'}{(2\varepsilon_a)^{3/2}(C+\xi')^{5/2}}\right|^2. \tag{5.6}$$

The expression for the heat flux is obtained by replacing $W^{5/2}$ in eq.(5.5) by $W^{7/2}$. Integration in eq.(5.6) can easily be carried out numerically

for given magnetic configuration, the derivative with respect to θ being calculated numerically by finite difference scheme.

For the case of $\varepsilon_H \ll \varepsilon_T$, eq.(3.20) can be expanded as

$$I(C,\xi) = \frac{2\varepsilon_H}{\varepsilon_T}\left\{A_0 H_0(\xi) + A_1 H_1(\xi) + \cdots\right\}, \tag{5.7}$$

with $A_0 = 1 - a_1 + a_2 - \cdots$, $A_1 = a_1 - 8a_2 + \cdots$. If we retain only the first term in the brace of eq.(5.7), and make the same kind of approximation for M, then the dependence of I_* and I_{**} to ξ and θ is separated, and we can obtain much simpler expression

$$S^{geo} = \int_0^{2\pi} \frac{d\theta}{2\pi} \frac{\varepsilon_H^{3/2}}{\varepsilon_T^{11/2}} A_0 \left\{ \frac{16}{9}\left(\frac{\partial \varepsilon_T}{\partial \theta}\right)^2 - \frac{32}{15}\frac{\partial \varepsilon_H}{\partial \theta}\frac{\partial \varepsilon_T}{\partial \theta} + 0.684\left(\frac{\partial \varepsilon_H}{\partial \theta}\right)^2 \right.$$

$$\left. + 0.804\left(\frac{\varepsilon_H}{A_0}\frac{\partial A_0}{\partial \theta}\right)^2 - 2\frac{\varepsilon_H}{A_0}\frac{\partial A_0}{\partial \theta}\left[\frac{256}{225}\frac{\partial \varepsilon_T}{\partial \theta} - 0.625\frac{\partial \varepsilon_H}{\partial \theta}\right] \right\}. \tag{5.8}$$

When $\partial A_0/\partial\theta = 0$ and $\varepsilon_T \sim 1$, eq.(5.8) becomes to the expression given in Ref.4. The factor $\varepsilon_\dagger^{11/2}$ in the denominator in eq.(5.8) may have significant effects in the low aspect torus.

Comparison of eq.(5.8) with the result of direct integration of eq.(5.6) shows that the geometrical factor (5.8) gives good approximation near the magnetic axis, where ε_H is small, as is expected; but in the outer region where ε_H is not small they give substantial differences.

§6. Numerical Results

A. Magnetic Configurations

First we will briefly describe the vacuum magnetic fields used in the following calculations. The typical fields are those used in the LHS

configuration study: toroidal period number N=10, the major radius R_c=4m, and averaged field strength B_0=4T. The configurations with N=8, 12 and 14 are also investigated. The magnetic field is expressed as the sum of the two parts, the three dimensional field produced by helical coils, and the additional axisymmetric poloidal field. The magnetic field is calculated by the Bio-Savart's law for the finite size helical coil.[11] The helical coils are wound around the torus

$$r = R_c - a_c \cos\theta, \quad z = a_c \sin\theta, \tag{6.1}$$

with the winding law

$$\theta = \kappa\varphi - \alpha \sin(\kappa\varphi), \quad \kappa \equiv \frac{N}{l}, \tag{6.2}$$

where (r,φ,z) are the cylindrical coordinates, and l=2 is the polarity of the helical coils. The pitch parameter γ_c is defined as

$$\gamma_c \equiv \frac{\kappa a_c}{R_c}. \tag{6.3}$$

The helical coil has finite size corresponding to coil current density j_c = 4kA/cm^2 for N=10, and 8. For N=12 and 14 configurations j_c=5.3kA/cm^2 is assumed. The concrete form of the size and cross section of the helical coil is given in Ref.12. The effects of the size of the helical coils are not important in the range of 3 to 5kA/cm^2 in the following analyses, except for the position of the wall, which is placed 15cm distant from the coil surface.

As the poloidal field, the analytic expression in terms of multipole expansion is used.

$$\Psi^{pol}(r,z) = \frac{B_v}{2}(r^2-R_c^2) + \frac{B_Q}{8}\{4r^2z^2-(r^2-R_c^2)^2\}$$
$$+\frac{B_H}{24}\{8r^2z^4-12r^2(r^2-R_c^2)z^2+(r^2-R_c^2)^3\}+\cdots, \tag{6.4}$$

with

$$B_r^{pol} = -B_0 \frac{\partial \Psi^{pol}}{\partial z}, \quad B_z^{pol} = B_0 \frac{\partial \Psi^{pol}}{\partial r}. \tag{6.5}$$

The helical coil produces not only the helical field, but also multiplole field components. The applied vertical field B_V is measured by the position of the magnetic axis $\Delta_0 \equiv R_{axis}-R_c$, while the quadrupole field B_Q is measured by the percentage of the cancellation of the quadrupole component of the field produced by the helical coils. The hexapole field and higher components are set to zero. When the quadrupole component is 100% cancelled (*i. e.* B_Q=100%), the shape of the averaged surface is nearly circular. When B_Q < 100%, the averaged surface is vertically elongated, while it is horizontally elongated when B_Q > 100%.

The outermost surface is determined by tracing about 40 lines of force starting from φ=0, z=0.

For the sake of understanding of the magnetic surface properties in these parameters, the change of the mean radius, rotational transform at the surface, and the depth of the magnetic well in the position of the magnetic axis (Δ_0) are shown in Fig.1 and Fig.2. The position of the last closed surface is affected by the presence of island, which causes the unusual dependence of the surface quantities depending on the last closed surface (for instance, at Δ_0=-10cm, for B_Q=100%, α=0, and at Δ_0=-7.5cm, for B_Q=100%, α=0.2).

The typical structure of ε_T, ε_H, α_1, α_2, α_3 is shown in Fig.3 and 4. The values of α_1 is from 0.1 to 0.15 for the cases studied. As n increases, the value of α_n decreases gradually. The main structure of the magnetic field is almost fixed in space and the shift of the magnetic surface changes the relative position between that structure and the magnetic surface. Important is that as the result of inward shift the

helical ripple changes from 0.15 to 0.4. This change is almost ignored in the past analyses based on the model magnetic field. The magnetic field strength is not harmonic in toroidal direction, and this may have significant effects to particle orbit especially in the outer region.

We shall note that the contours of B_{max} = constant and B_{min}= constant are nearly circular in these cases, because the cross section of the surface on which the helical coils are wound is circular (see eq.(6.1)).

B. Outermost loss-free surface

In the following analysis, no electric field is assumed. Some examples of the orbit, which determines the radius of the loss-free surface, are shown in Fig.5. The dependence of $r_L/a_p \equiv (\psi_L/\psi_b)^{1/2}$ to the shift of the magnetic axis is shown in Fig.6 and 8. The three curves are drawn for B_Q= 0,100,and 200% in Fig.6. The dependence with respect to B_Q is shown in Fig.7. The dip at B_Q=100% in the case of Δ_0=-10cm is due to the island near the surface. The case B_Q=100% seems to be optimum for wide range of axis position. Therefore, we will adopt B_Q=100% as the standard parameter.

As the plasma shifts inward, the radius of the loss-free surface determined by $v_{//}$=0 particles first increases; it is determined by the orbit crossing the outermost surface inside of the torus. When the shift becomes large, the radius begins to decrease; it is determined by the orbit crossing outermost surface outside the torus. For the case of B_Q=200%, since the averaged surface is horizontally elongated, the radius is limited by the orbit crossing the outermost surface at the top and bottom of the torus.

As for the blocked particles, the angle of the transition point θ_t

determining ψ_{Lt} moves inside as the shift increases. This angle θ_t is larger for the negative pitch modulation than for the positive pitch modulation.

Figure 8 shows the dependence of r_L/a_p to the shift of the magnetic axis for different values of pitch modulation. The curves for α=0 and 0.1 agree well with the more precise results in Ref.10, obtained by integrating drift equation of motion. The same is shown in Fig.9 with α as the abscissa.

These figures show that the inward shift significantly improves the particle confinement, especially in the case of α=0.1 and B_0 =100%. This is due to the fact that the plasma radius is large enough to that large shift in case of α=0.1 (a_p= 60cm for Δ_0=-30cm), while it decreases for the case of α=0.2 when $-\Delta_0 \geqq 20$cm.

The case of different N, with B_0=100% and α=0, is shown in Fig.10. Four curves correspond to N=8,10,12 and 14, with the pitch parameters 1.15,1.20,1.23 and 1.25, respectively. When the plasma shift is small,as N decreases the confinement become worse. However, if the inward shift of magnetic axis is sufficiently large, the particle confinement is improved in lower N configurations. Since the clearance between plasma and wall becomes less stringent in lower N (if R_c is fixed), the larger shift is possible; and the low aspect ratio may allow the larger inward shift without deteriorating MHD stability.

C. *Geometrical factor of 1/ν regime*

The geometric factor eq.(5.6) has strong dependence on the radius, $S^{geo} \propto p^4$ or p^5; hence the small change of plasma radius strongly affects its value.

Since D/ψ^2 is proportional to the particle confinement time, D being the diffusion coefficient, the ratio S^{geo}/ψ^2, padial dependence of which is much weaker than S^{geo} itself, may be taken as the parameter expressing the confinement property of the configuration. The value of S^{geo}/ψ^2 evaluated at the magnetic surface ψ/ψ_S=0.5 for the axis shift are plotted in Fig.11. The dependence for B_0 is shown in Fig.12. For five values of pitch modulation, the dependence on Δ_0 is shown in Fig.13 and 14. The dependence on N is shown in Fig.15, the parameters being same to Fig.10. The steep rise in the left side in Fig.15 is due to the reduction of the plasma radius, because the magnetic surface touches to the wall.

Thus, the significant improvement is caused by inward shift or negative pitch modulation, reflecting the improvement in particle orbit. The accuracy of eq.(5.8) is within factor 2 in this radius.

§7. Summary and Discussion

The analytic expression for the longitudinal adiabatic invariant for actual magnetic configuration will give a powerful method to study the particle orbit in toroidal helical system; it is also useful to investigate transport coefficients in $1/\nu$ regime.

In the LHS configuration study the improvement of particle orbit as well as the MHD beta limit in the lower pitch number is discovered.[8] The orbit loss can be significantly reduced by the sufficient amount of inward shift of the plasma and magnetic axis, or by applying negative pitch modulation of the helical coils. The negative pitch modulation, however, imposes severe restriction to the clearance between plasma and wall: the

improvement by inward shift in the negatively modulated coils is possible only in the device with lower magnetic field (smaller coil size) or larger dimension. As for the lower N, *i.e.* N=8, the inward shift up to 25cm improves the orbit, which seems to be compatible with MHD stability. Such low aspect device may be a hopeful candidate for the large experimental device.

The analyses done in this paper are only for the vacuum field. In finite beta plasmas, the deformation of the magnetic durface due to the Pfirsch - Schlüter current may degrade the particle confinement. The problem is left to the future study.

Acknowledgement

The author is grateful to Dr. H.Sanuki for his helpful discussions. The various ideas such as the improvement of particle confinement by inward shift of plasma, and employing the concept of the outermost loss-free surface as the characteristic number for the performance of the configuration, are born in the collaboration for the design study of the Large Helical Devices in the past three years, and the stimulating discussions in the Design Group of the Large Helical System. The author express his gratitude for the members of the Design Group; especially, discussions with Prof. T.Kamimura, Dr. H.Sanuki, Prof. M.Wakatani, and Dr. K.Hanatani are appreciated. This work is supported by Grant-in-Aid for Fusion Research of Ministry of Education, Science and Culture.

Appendix A. Calculation of Q in eqs.(3.6)

The integral for $\xi \leqq 1$

$$\mathbf{Q}(C;\xi) \equiv \int_0^{\frac{\pi}{2}} \frac{\xi \cos^2\theta d\theta}{\sqrt{1-\xi \sin^2\theta}}, \tag{A.1}$$

can be expressed in terms of the complete integral of the third kind.

$$\mathbf{Q}(C;\xi) \equiv \left(1+\frac{\xi}{C}\right)\Pi_1\left(\frac{\xi}{C};\xi\right)-\mathbf{K}(\xi) \qquad (\text{for } \xi<1), \tag{A.2}$$

The complete elliptic integral of the third kind can be represented in terms of the incomplete integrals of the first and second kind,[13]

$$F(\varphi,\xi) = \int_0^{\varphi} \frac{d\varphi}{\sqrt{1-\xi \sin^2\theta}}, \quad E(\varphi,\xi) = \int_0^{\varphi} \sqrt{1-\xi \sin^2\theta}\, d\varphi. \tag{A.3}$$

Since $\nu=\xi/C>0$, it is convenient to use the following expression

$$\mathbf{Q}(C;\xi)=\left[\frac{C+\xi}{C(C+1)}\right]^{1/2}\left\{\mathbf{E}(\xi)F(\varphi,1-\xi)-\mathbf{K}(\xi)\left[F(\varphi,1-\xi)-E(\varphi,1-\xi)\right]\right\}$$

$$-\frac{1-\xi}{C+1}\mathbf{K}(\xi) \qquad (\xi \leqq 1), \tag{A.4}$$

where

$$\varphi = \arctan\frac{1}{C^{1/2}}. \tag{A.5}$$

Similarly, eq.(3.6b) for $\xi \geqq 1$ can be expressed as

$$\mathbf{Q}(C;\xi)=\left[\frac{C+\xi}{C(C+1)}\right]^{1/2}\left\{\mathbf{E}\left(\frac{1}{\xi}\right)F\left(\varphi,1-\frac{1}{\xi}\right)-\mathbf{K}\left(\frac{1}{\xi}\right)\left[F\left(\varphi,1-\frac{1}{\xi}\right)-E\left(\varphi,1-\frac{1}{\xi}\right)\right]\right\}, \tag{A.6}$$

with

$$\varphi = \arctan\left(\frac{\xi}{C}\right)^{1/2}. \tag{A.7}$$

When $\varepsilon_H \ll \varepsilon_T$, we can approximate that $C^{-1} \simeq \varepsilon_H/\varepsilon_T \ll 1$, and we have

$$Q(C;\xi) \sim \frac{1}{C}H_0(\xi) - \frac{1}{C^2}H_1(\xi) + \ldots, \tag{A.8}$$

In calculating incomplete elliptic integrals the ascending Landen transformation

$$k_{n+1}' = \frac{1-k_n}{1+k_n}, \qquad k_{n+1}^2 = 1-(k_{n+1}')^2,$$

$$\varphi_{n+1} = \frac{1}{2}\{\varphi_n + \arcsin(k_n \sin\varphi_n)\}, \tag{A.9}$$

is useful to change the modulus to increase, until the formulae

$$F(\varphi,1) = \log\tan\left(\frac{\varphi}{2}+\frac{\pi}{4}\right), \qquad E(\varphi,1) = \sin\varphi, \tag{A.10}$$

can be used. Then the recurrence formulae

$$F(\varphi_n,k_n^2) = (1+k_{n+1}')F(\varphi_{n+1},k_{n+1}^2),$$

$$E(\varphi_n,k_n^2) = \frac{2}{1+k_{n+1}}\{2E(\varphi_{n+1},k_{n+1}^2) + k_{n+1}'F(\varphi_{n+1},k_{n+1}^2)\} - k_n\sin\varphi_n, \tag{A.11}$$

are used to calculate the sought functions. Less than 10 iterations are sufficient to obtain 10 significant digit, except for the case of $k=\xi^{1/2}<10^{-10}$, where $F(\varphi,0)=E(\varphi,0)=\varphi$, are used instead.

Appendix B. Calculation of M in eq.(5.3)

We shall consider the following integral

$$J(C,\xi) = \int_0^{\frac{\pi}{2}} \frac{\xi\cos^2\theta}{(C+\xi\sin^2\theta)^2\sqrt{1-\xi\sin^2\theta}} \times\left\{1+\sum_{n=0}^{\infty}(-1)^n a_n T_n(1-2\xi\sin^2\theta)\right\}d\theta, \tag{B.1}$$

for the case of $\xi \leqq 1$. Then eq.(5.3) can be written as

$$M = \frac{4R_0}{N}\left(\frac{m\mu}{B_0\varepsilon_H^3}\right)^{1/2} J(C,\xi). \tag{B.2}$$

We introduce the function

$$\mathbf{Q}_1(C;\xi) \equiv \int_0^{\frac{\pi}{2}} \frac{\xi\cos^2\theta d\theta}{(C+\xi\sin^2\theta)^2\sqrt{1-\xi\sin^2\theta}}, \tag{B.3}$$

which is related to $\mathbf{Q}$, defined in eq.(A.1) or (3.6), by the relation

$$2C(C+1)(C+\xi)\mathbf{Q}_1(C,\xi) = \{C^2+(2C+1)\xi\}\mathbf{Q}(C,\xi)+(C+2)\mathbf{H}_0(\xi)-3\mathbf{H}_1(\xi). \tag{B.4}$$

Since $J=-\partial I/\partial C$ and $\mathbf{Q}_1=-\partial\mathbf{Q}/\partial C$, I being defined in eq.(3.12), we have the expression

$$J(C,\xi) = \left\{1+\sum_{n=1}^{\infty}(-1)^n a_n T_n(1+2C)\right\}\mathbf{Q}_1(C;\xi) - 2\sum_{n=1}^{\infty}(-1)^n a_n T_n'(1+2C)\mathbf{Q}(C;\xi)$$

$$-\sum_{n=2}^{\infty}\sum_{k=0}^{n-2}(-1)^n a_n g_{n,k}'(C)\mathbf{H}_k(\xi). \tag{B.5}$$

Here $'$ stands for the differentiation with respect to its argument, and the coefficients $g_{n,k}'$ can be calculated by using the recurrence relations:

$$g_{n+1,m}' = \begin{cases} 2g_{n,m}' - 4g_{n,m-1}' - g_{n-1,m}' & (\text{for } m\geq 1), \\ 2g_{n,0}' - g_{n-1,0}' - 8T_n'(1+2C) & (\text{for } m=0). \end{cases} \tag{B.6}$$

with

$$g'_{1,0} = 0, \quad g'_{2,1} = 0, \quad g'_{2,0} = -8. \tag{B.7}$$

REFERENCES

1) R.J.Hastie,J.B.Taylor, and F.A.Haas: Ann. Phys. (N.Y.) 41 (1967) 302

2) D.Dobrott and E.A.Frieman: Phys. Fluids 14 (1971) 349

3) M.Wakatani,S.Kodama,M.Nakasuga and K.Hanatani: Nucl. Fusion 21 (1981) 175

4) K.C.Shaing and S.A.Hokin: Phys. Fluids 26 (1983) 2136

5) J.R.Cary,C.L.Hedrick and J.S.Tolliver: Phys. Fluids 31 (1988) 1586

6) J.Todoroki: to be published.

7) Design Group for the New Large Helical System Device: *New Large Helical System Device*,(The Planning Office for New Institute for Fusion Plasma Science, Nagoya University, Nagoya, 1988)

8) J.Todoroki,T.Kamimura,H.Sanuki,T.Amano,T.Hayashi,K.Suzuki, T.Sato, K.Hanatani, Y.Nakamura, W.Wakatani and A.Iiyoshi: 12th Int. Conf. on Plasma Physics and Controlled Nuclear Fusion, Nice, 1988, IAEA-CN-50/C-5-4

9) A.Boozer: Phys. Fluids 24 (1981) 1999

10) K.Hanatani,H.Sanuki and T.Kamimura: *Basic Design of Large Helical Device*, Report of Design Group of Large Helical Device, (NIFS, Nagoya, 1989) p.584 [in Japanese]

11) J.Todoroki: Kakuyugo Kenkyu 57 (1987) 318 [in Japanese]

12) *Basic Design of Large Helical Device*, Report of Design Group of Large Helical Device, (NIFS, Nagoya, 1989) p.635 [in Japanese]

13) L.M.Milne-Thomson: *Handbook of Mathematical Functions*, edited by M. Abramowitz and I. Stegun, (Dover Publications, N.Y., 1964) p.587

Figure Captions

Fig.1 The magnetic surface properties with respect Δ_0, for the case N=10, γ_c=1.20, α= 0.

○: B_Q=0%; △: B_Q=100%; +: B_Q=200%

Fig.2 The magnetic surface properties with respect Δ_0. for the case N=10, γ_c=1.20, B_Q=100%.

○ : α=-0.2; △ : α=-0.1; + : α= 0; × : α= 0.1; □ : α=0.2.

Fig.3 The structure of ε_T,ε_H, a_1, a_2. The case is N=10, γ_c=1.20, α=0, B_Q=100%, and Δ_0=0.

Fig.4 The structure of ε_T,ε_H, a_1, a_2. The case is N=10, γ_c=1.20, α=0.1, B_Q=100%, and Δ_0=-35cm.

Fig.5 Examples of the orbit determines outermost loss-free surface for N=10. The bold line shows the orbit for transition particles, while the broken lines for $v_{\parallel}$=0 particles.

a) α= 0, Δ_0=-10cm; b) α= 0, Δ_0=-25cm; c) α=-0.2, Δ_0=-25cm.

Fig.6 Radius of loss-free surface versus position of magnetic axis Δ_0, for N=10, γ_c=1.20, and α=0.

○ : B_Q=0%; △ : B_Q=100%; + : B_Q=200%.

Fig.7 Radius of loss-free surface versus position of magnetic on the quadrupole field B_Q, for N=10, γ_c=1.20, and α=0.

○ : Δ_0= 0cm; △ : Δ_0=-10cm; + : Δ_0=-20cm; × : Δ_0=-30cm.

Fig.8 Radius of loss-free surface versus position of magnetic axis Δ_0, on the position of magnetic axis, for N=10, γ_c=1.20, and B_Q=100%.

○ : α=-0.2; △ : α=-0.1; + : α= 0; × : α= 0.1; □ : α=0.2.

Fig.9 Radius of loss-free surface versus position of magnetic on the parameter α of pitch modulation, for N=10, γ_c=1.20, and B_Q=100%.

○ : Δ_0= 0; △ : Δ_0=-10cm; + : Δ_0=-20cm; × : Δ_0=-30cm.

Fig.10 Radius of loss-free surface versus position of magnetic axis Δ_0 for α=0, and B_Q=100%.

○ : N=8, γ_c=1.15, j_c= 4kA/cm^2; △ : N=10, γ_c=1.20, j_c= 4kA/cm^2; + : N=12, γ_c=1.23, j_c=5.3kA/cm^2; × : N=14, γ_c=1.25, j_c=5.3kA/cm^2.

Fig.11 Dependence of S^{geo}/ψ^2 at ψ/ψ_S=0.5 on the position of magnetic axis, for N=10, γ_c=1.20, and α=0.

○ : B_Q=0%; △ : B_Q=100%; + : B_Q=200%

Fig.12 Dependence of S^{geo}/ψ^2 at ψ/ψ_S=0.5 on the quadrupole field B_Q, for N=10, γ_c=1.20 and α=0.

○ : Δ_0= 0cm; △ : Δ_0=-10cm; + : Δ_0=-20cm; × : Δ_0=-30cm.

Fig.13 Dependence of S^{geo}/ψ^2 at ψ/ψ_S=0.5 on the position of magnetic axis, for N=10, γ_c=1.20 and B_Q=100%.

○ : α=-0.2; △ : α=-0.1; + : α= 0; × : α= 0.1; □ : α=0.2.

Fig.14 Dependence of S^{geo}/ψ^2 at ψ/ψ_S=0.5 on the parameter α of pitch modulation, for N=10, γ_c =1.20 and B_Q=100%.

○ : Δ_0= 0cm; △ : Δ_0=-10cm; + : Δ_0=-20cm; × : Δ_0=-30cm.

Fig.15 Dependence of S^{geo}/ψ^2 at ψ/ψ_S=0.5 for α=0, and B_Q=100%.

○ : N=8, γ_c=1.15, j_c=4kA/cm^2; △ : N=10, γ_c=1.20, j_c=4kA/cm^2;

+ : N=12, γ_c=1.23, j_c=5.3kA/cm^2; × : N=14, γ_c=1.25, j_c=5.3kA/cm^2.

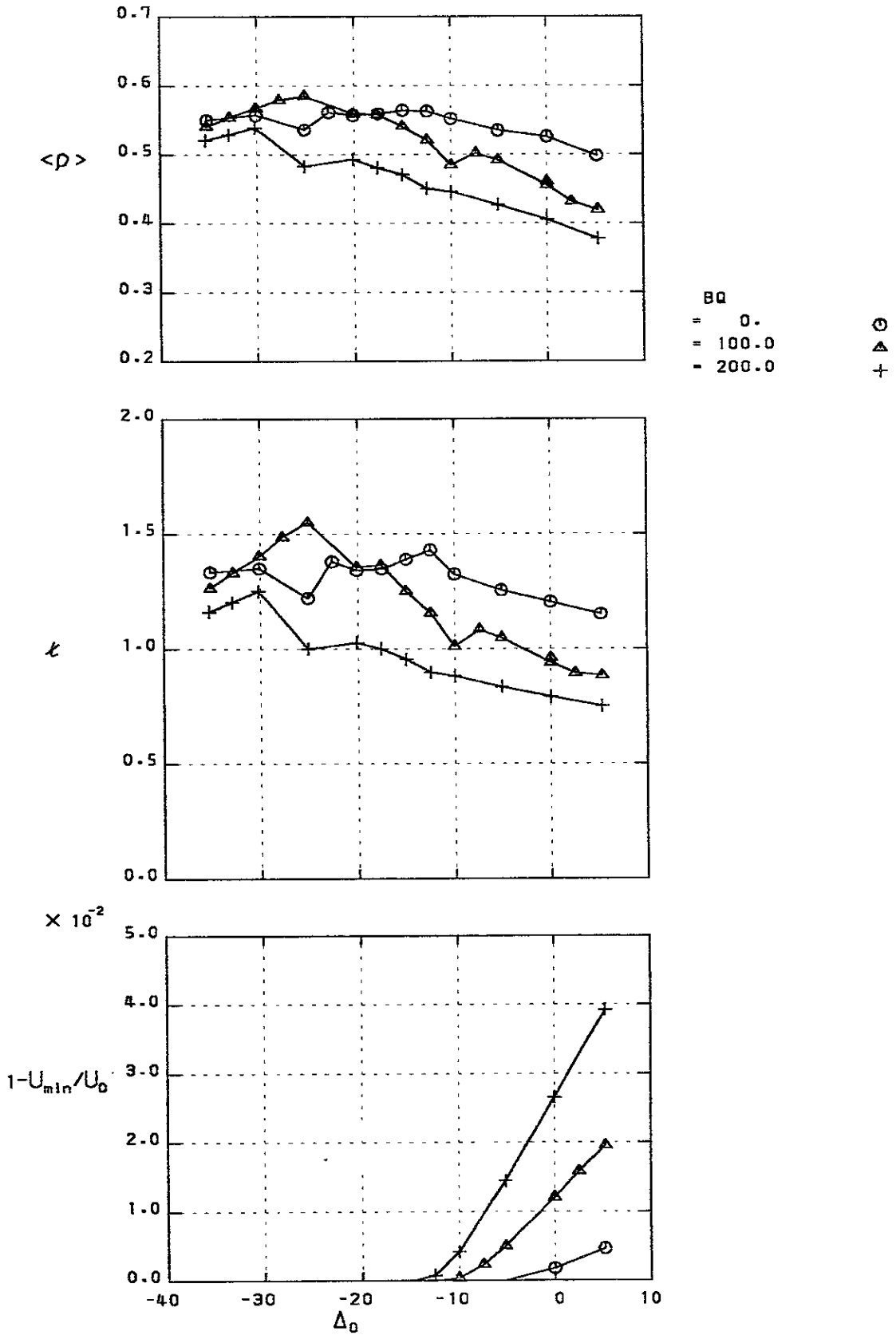
<ρ>
0.7
0.6
0.5
0.4
0.3
0.2
BQ
= 0.
= 100.0
= 200.0
t
2.0
1.5
1.0
0.5
0.0
× 10⁻²
1-Umin/U0
5.0
4.0
3.0
2.0
1.0
0.0
-40
-30
-20
-10
0
10
Δ0

Fig.1

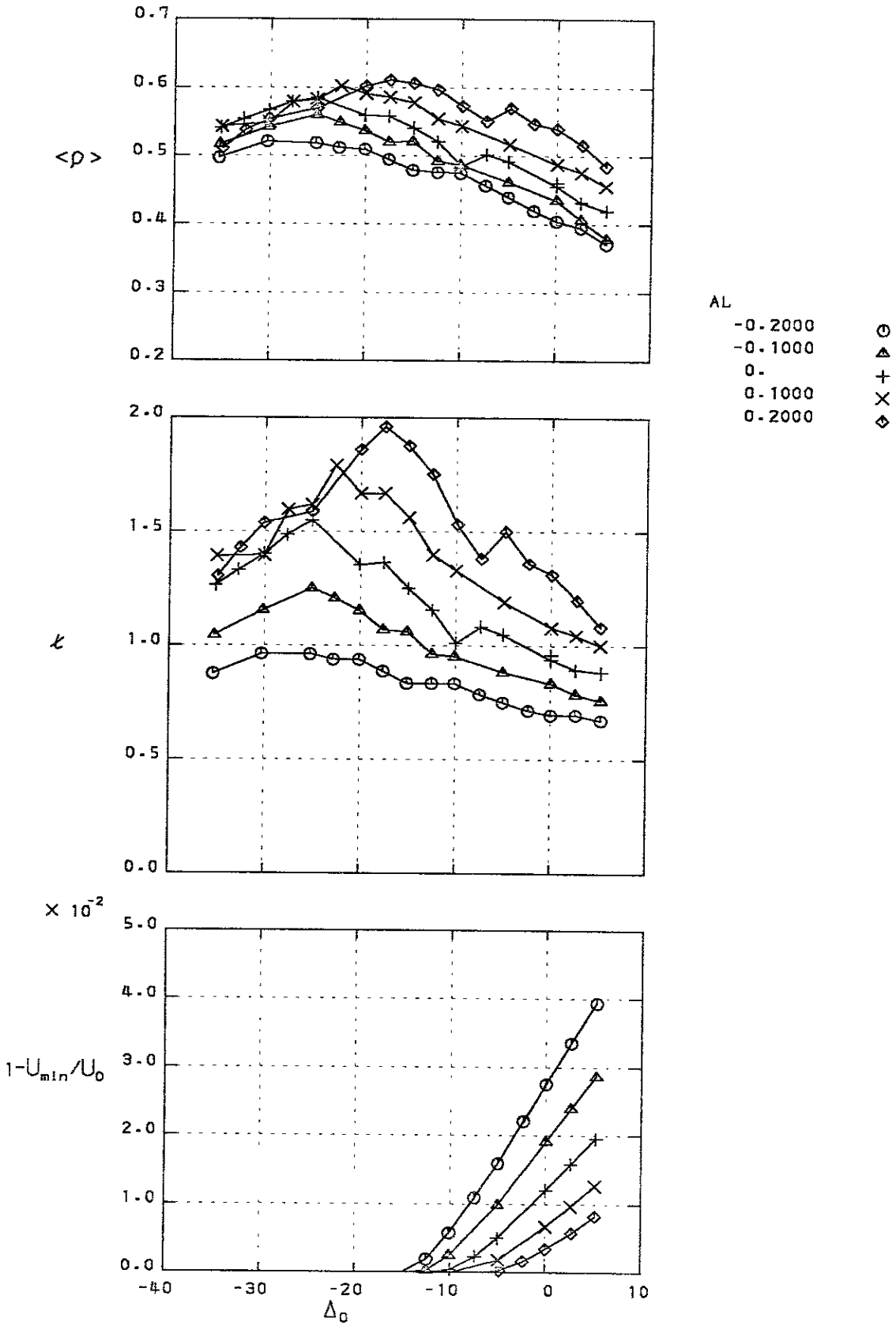
0.7
0.6
0.5
0.4
0.3
0.2
<ρ>
AL
-0.2000
-0.1000
0.
0.1000
0.2000
2.0
1.5
1.0
0.5
0.0
ℓ
× 10⁻²
5.0
4.0
3.0
2.0
1.0
0.0
1-U_min/U_0
-40
-30
-20
-10
0
10
Δ_0

Fig.2

NAME - M10G20#S.P0
MGS@ - MGS0/M10G20#.006.03

M10G20#S.P0

Bvert = 0.3039 (101.85) Delta = -0.101
Bquad = 0.0209 (100.00)
Bhexa = 0.0000 (0.00)
Bocta = 0.0000 (0.00)

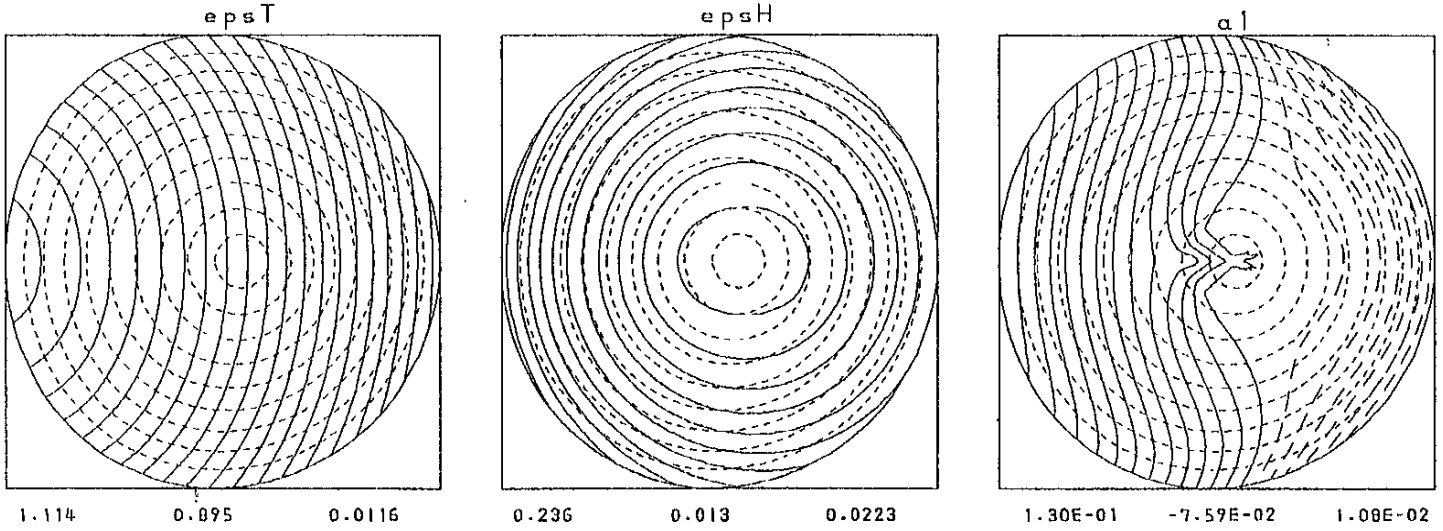

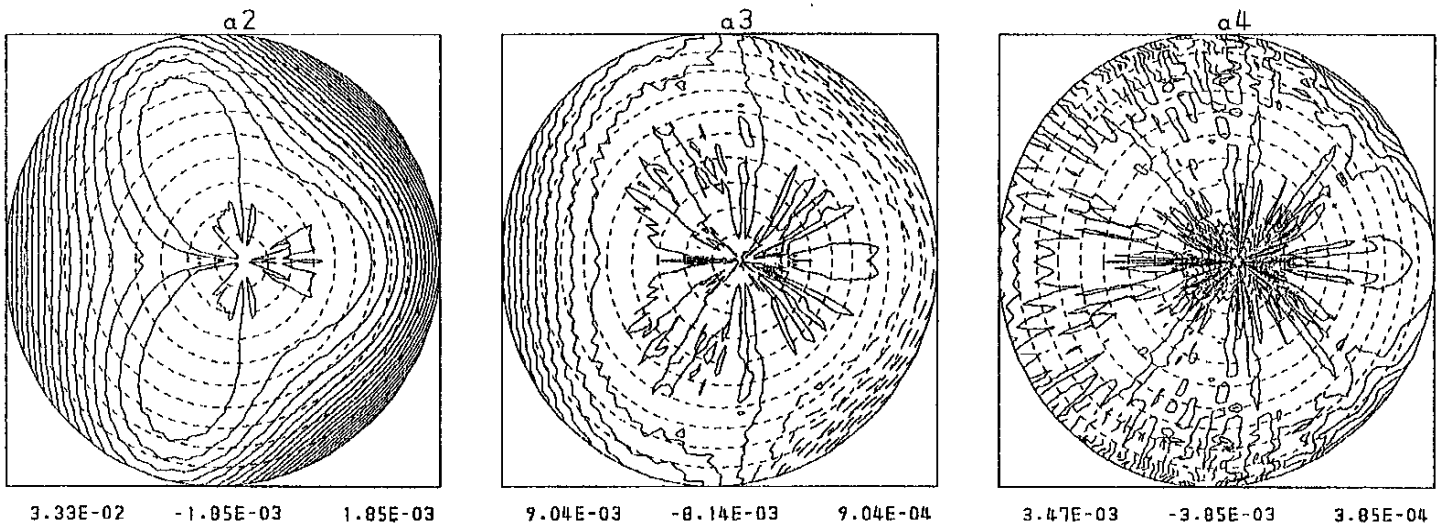

Fig.3

MAGNI/V-3.0(89-08-28) *M10G20#S.P0.Q100 *89-11-09 M10G20#.006

NAME - M10G20#S.P1
MGS@ - MGS@/M10G20#.000.00

M10G20#S.P1

Bvert = 0.2916 (113.14) Delta = -0.349
Bquad = 0.0202 (100.00)
Bhexa = 0.0000 (0.00)
Bocta = 0.0000 (0.00)

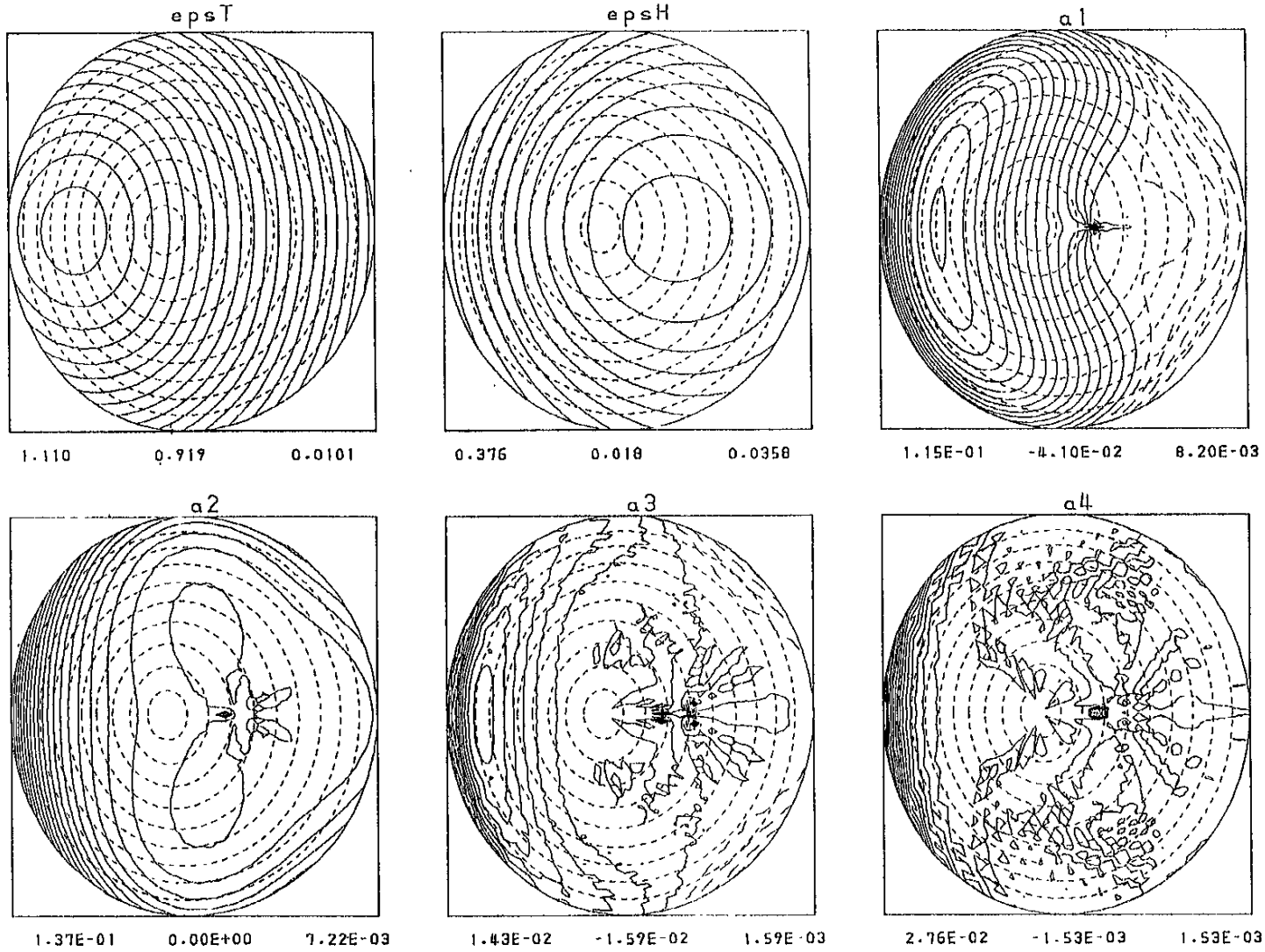

Fig.4

MAGN1/V-3.0(89-08-28) *M10G20#S.P1 *89-11-10 M10G20#.000

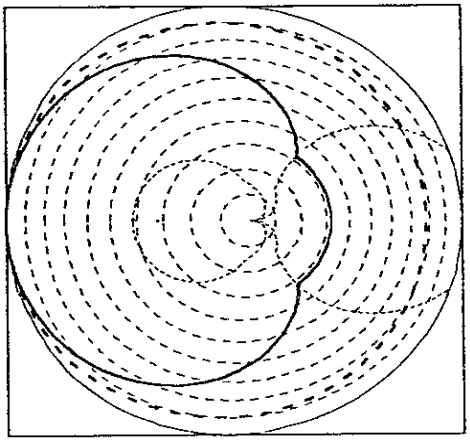

a) $\alpha = 0$, $\Delta_0 = -10cm$

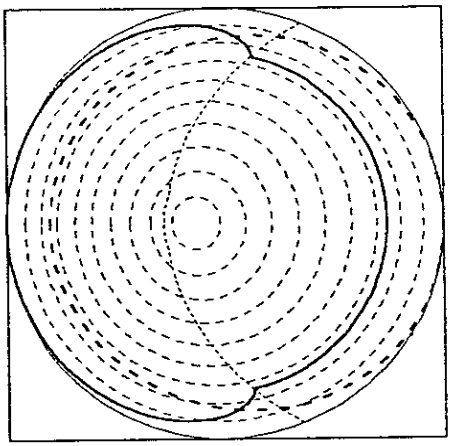

b) $\alpha = 0$, $\Delta_0 = -25cm$

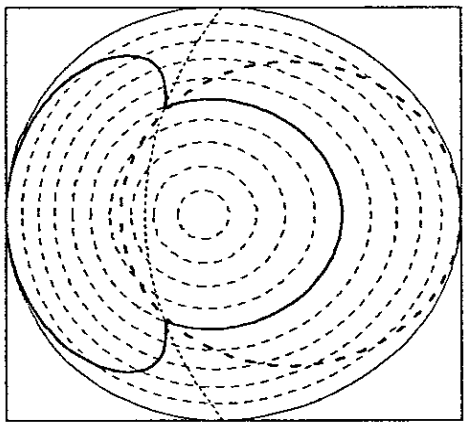

c) $\alpha = -0.2$, $\Delta_0 = -25cm$

Fig.5

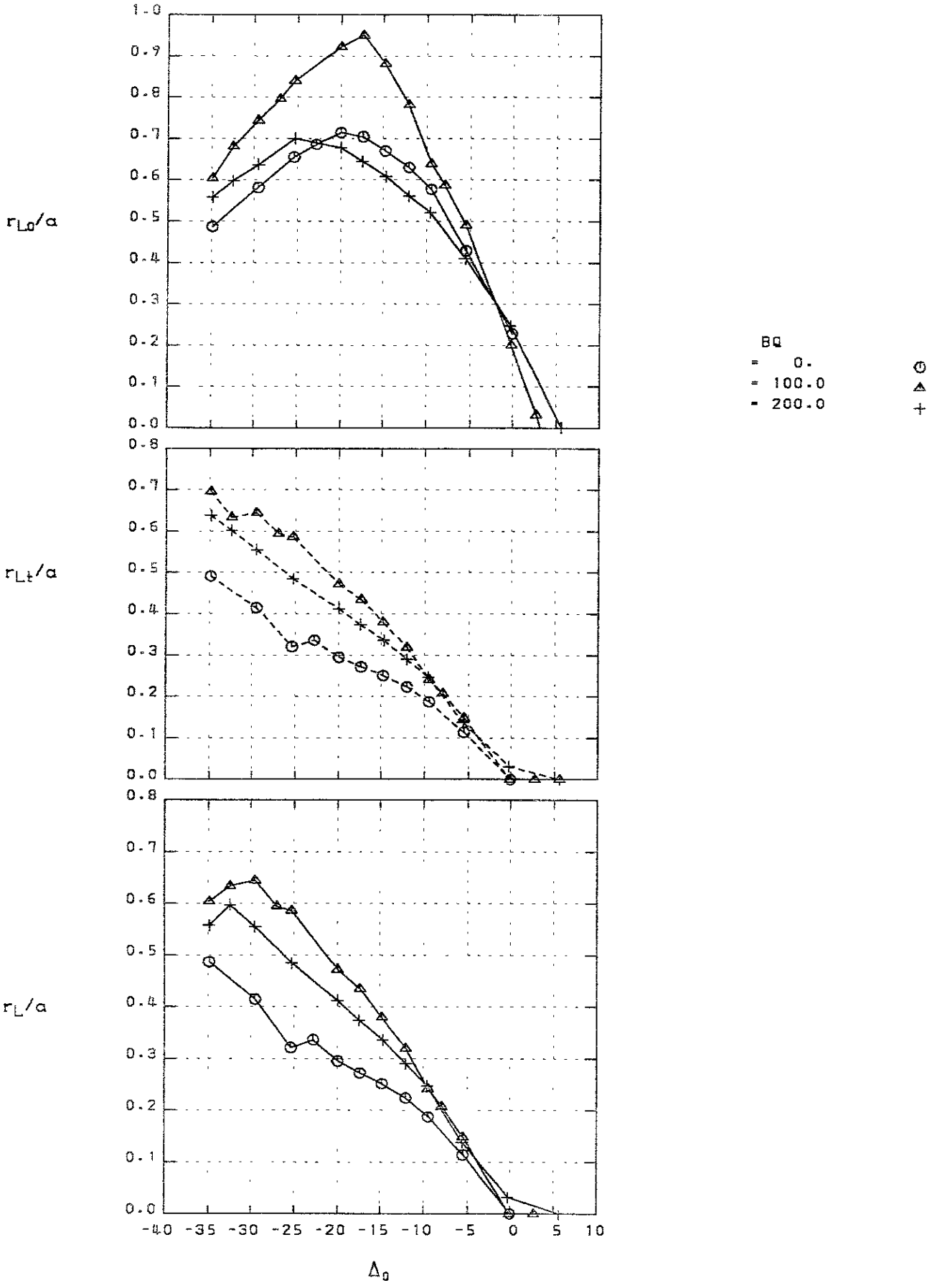
r_{Lo}/a
r_{Lt}/a
r_L/a
1.0
0.9
0.8
0.7
0.6
0.5
0.4
0.3
0.2
0.1
0.0
-40 -35 -30 -25 -20 -15 -10 -5 0 5 10
Δ_0
BQ
= 0.
= 100.0
= 200.0

Fig.6

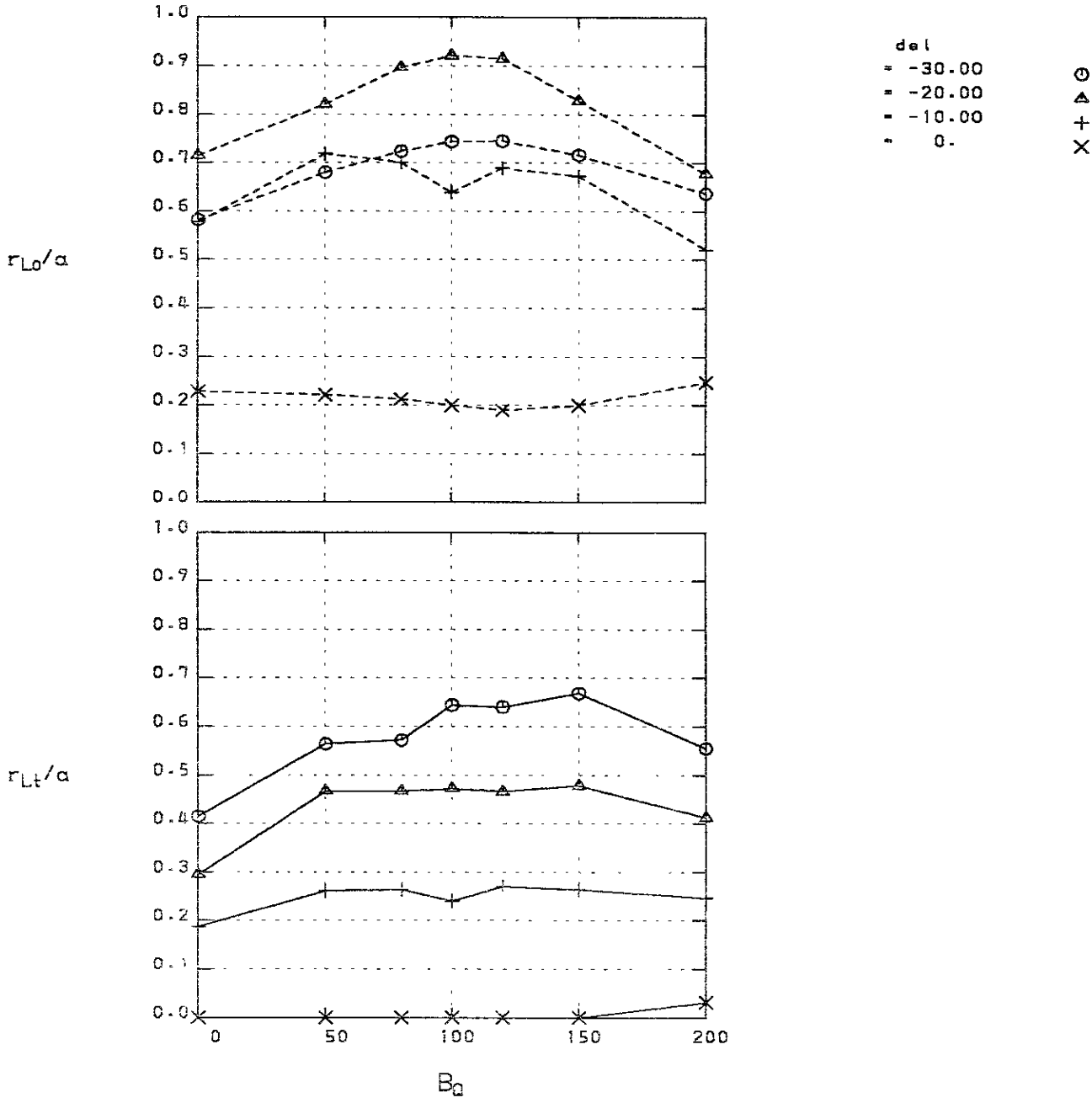
del
= -30.00
= -20.00
= -10.00
= 0.
r_{Lo}/a
r_{Lt}/a
1.0
0.9
0.8
0.7
0.6
0.5
0.4
0.3
0.2
0.1
0.0
0
50
100
150
200
B_a

Fig 7

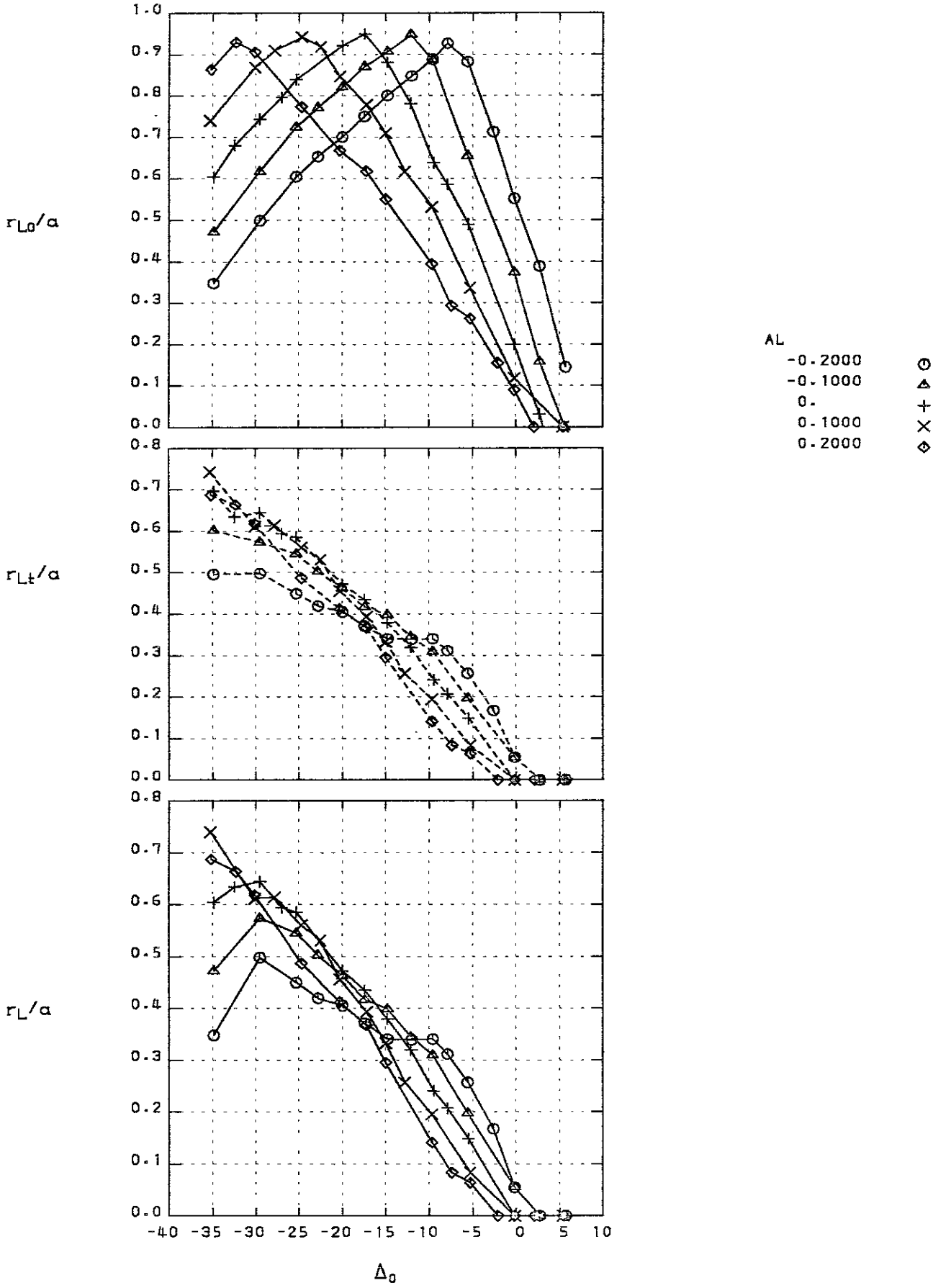
r_{L0}/a
r_{Lt}/a
r_L/a
1.0
0.9
0.8
0.7
0.6
0.5
0.4
0.3
0.2
0.1
0.0
-40 -35 -30 -25 -20 -15 -10 -5 0 5 10
Δ_0
AL
-0.2000
-0.1000
0.
0.1000
0.2000

Fig.8

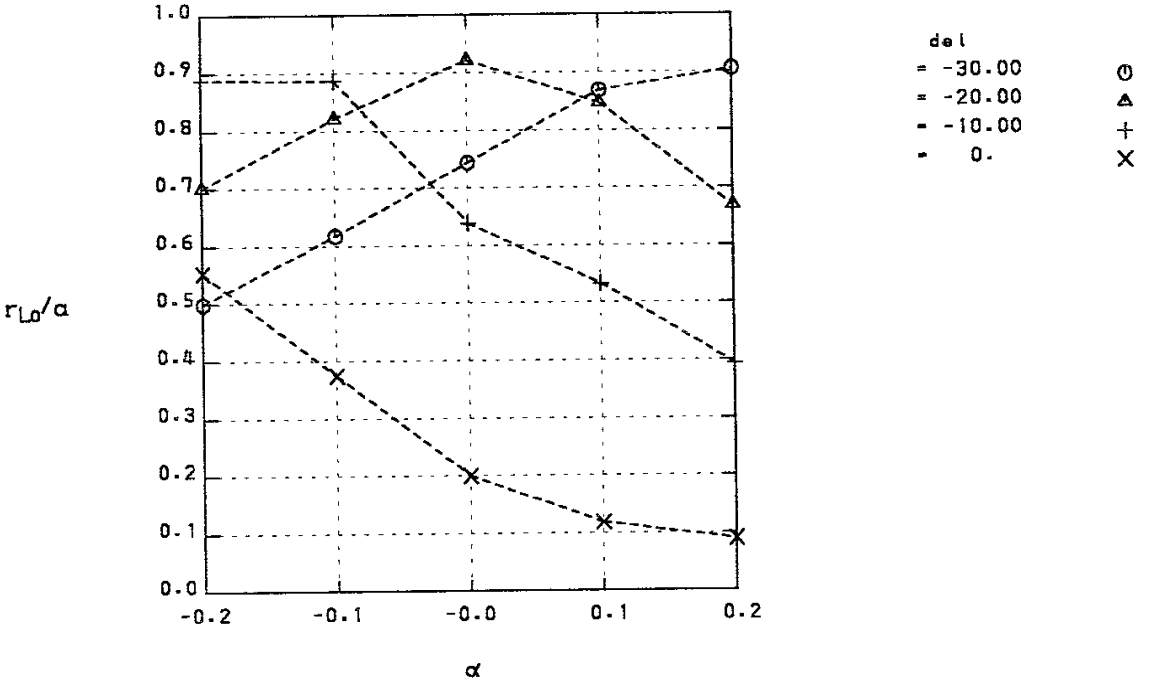
del
= -30.00
= -20.00
= -10.00
= 0.
r_{Lo}/a
1.0
0.9
0.8
0.7
0.6
0.5
0.4
0.3
0.2
0.1
0.0
-0.2
-0.1
-0.0
0.1
0.2
α

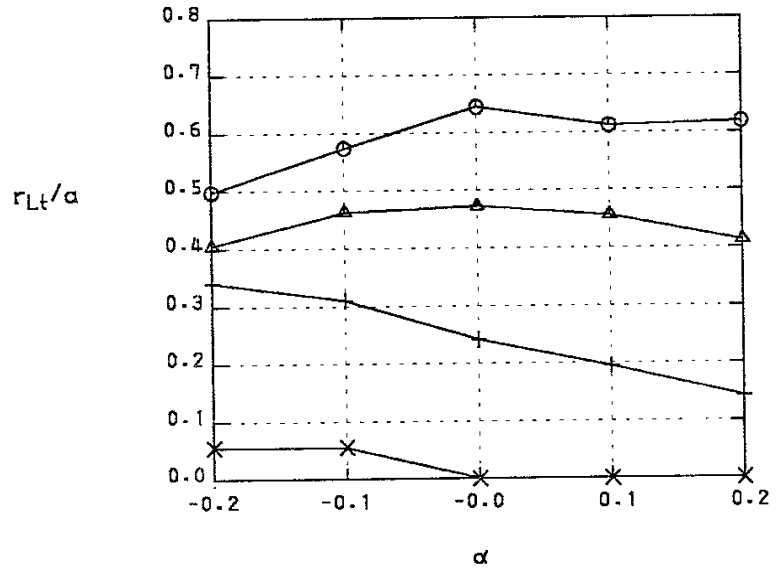
r_{Lt}/a
0.8
0.7
0.6
0.5
0.4
0.3
0.2
0.1
0.0
-0.2
-0.1
-0.0
0.1
0.2
α

Fig.9

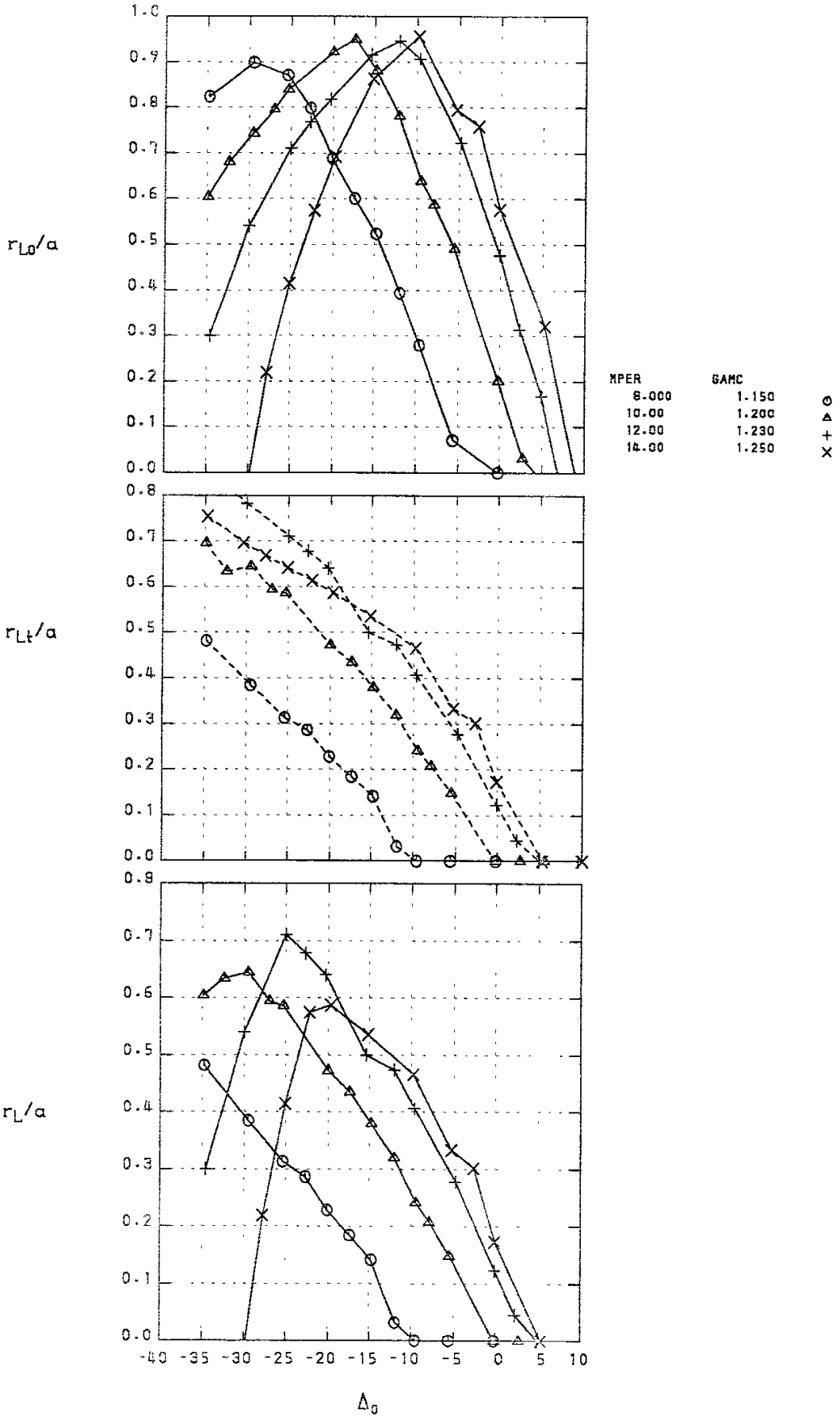
r_{L0}/a
r_{Lt}/a
r_L/a
MPER GAMC
8.000 1.150
10.00 1.200
12.00 1.230
14.00 1.250
Δ_0

Fig.10

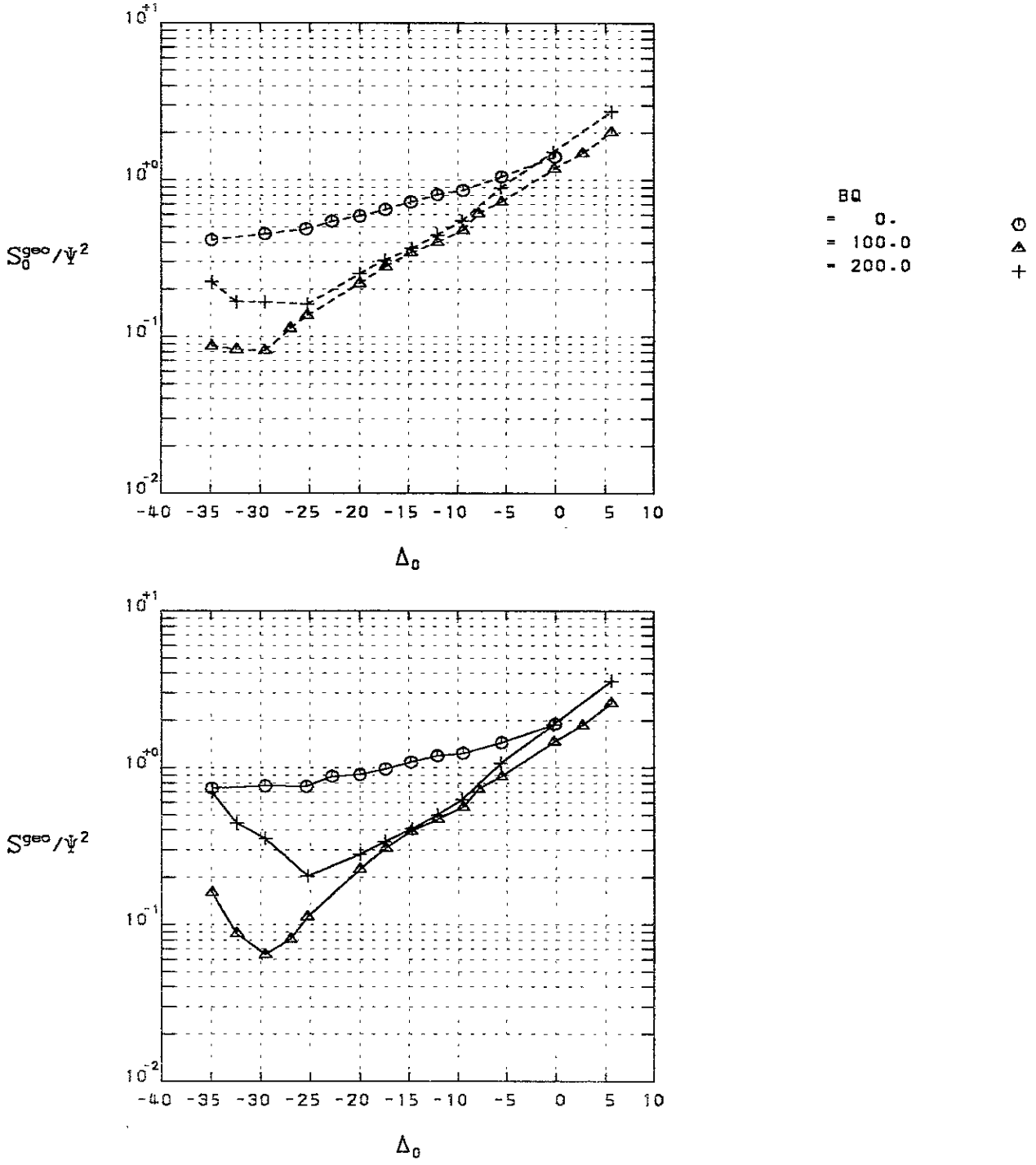
S_0^{geo}/Ψ^2
10^{+1}
10^{+0}
10^{-1}
10^{-2}
-40 -35 -30 -25 -20 -15 -10 -5 0 5 10
Δ_0
BQ
= 0.
= 100.0
= 200.0
S^{geo}/Ψ^2
10^{+1}
10^{+0}
10^{-1}
10^{-2}
-40 -35 -30 -25 -20 -15 -10 -5 0 5 10
Δ_0

Fig.11

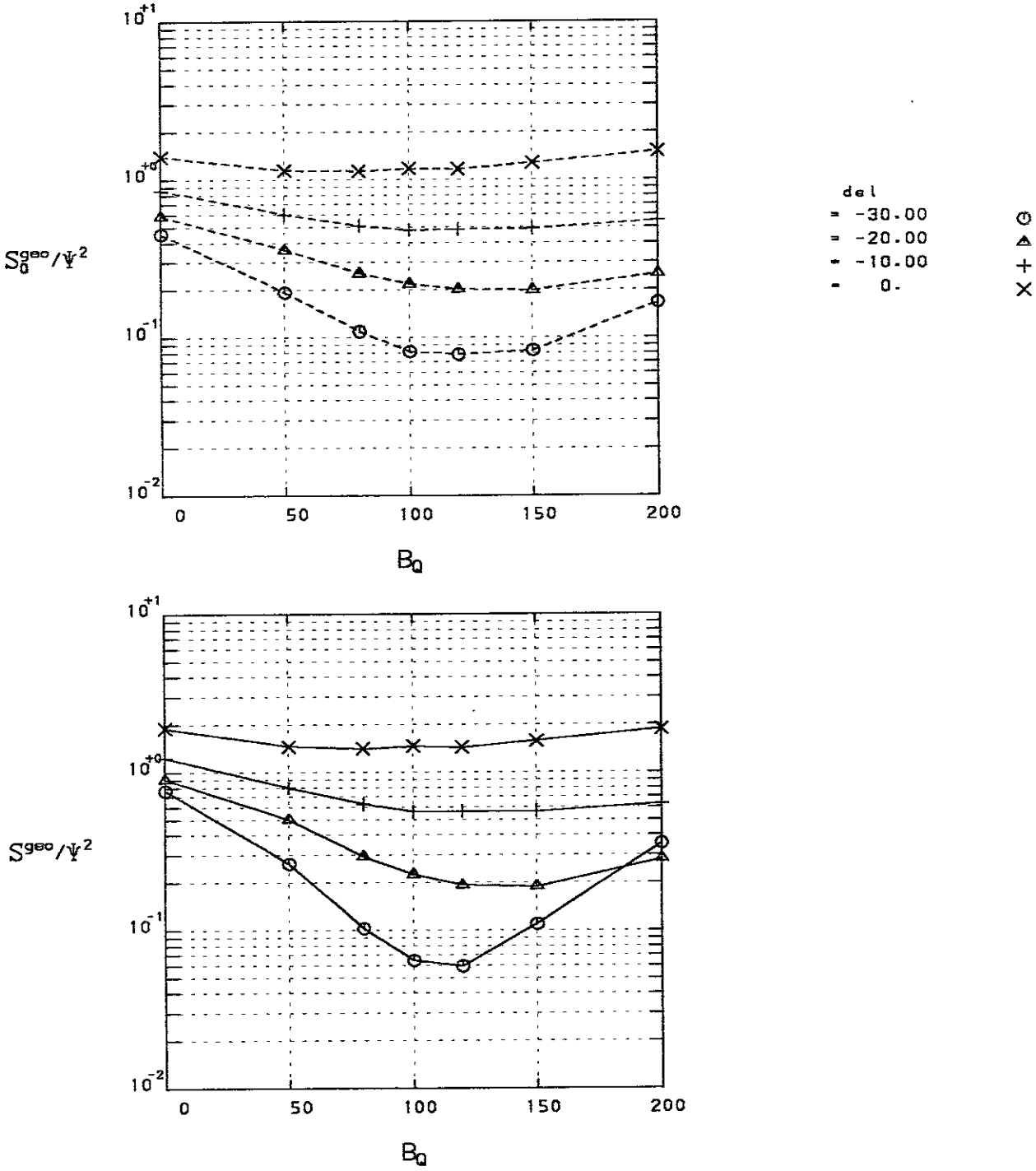
S_0^{geo}/Ψ^2
10^{+1}
10^{+0}
10^{-1}
10^{-2}
0
50
100
150
200
B_Q
del
= -30.00
= -20.00
= -10.00
= 0.
S^{geo}/Ψ^2
10^{+1}
10^{+0}
10^{-1}
10^{-2}
0
50
100
150
200
B_Q

Fig. 12

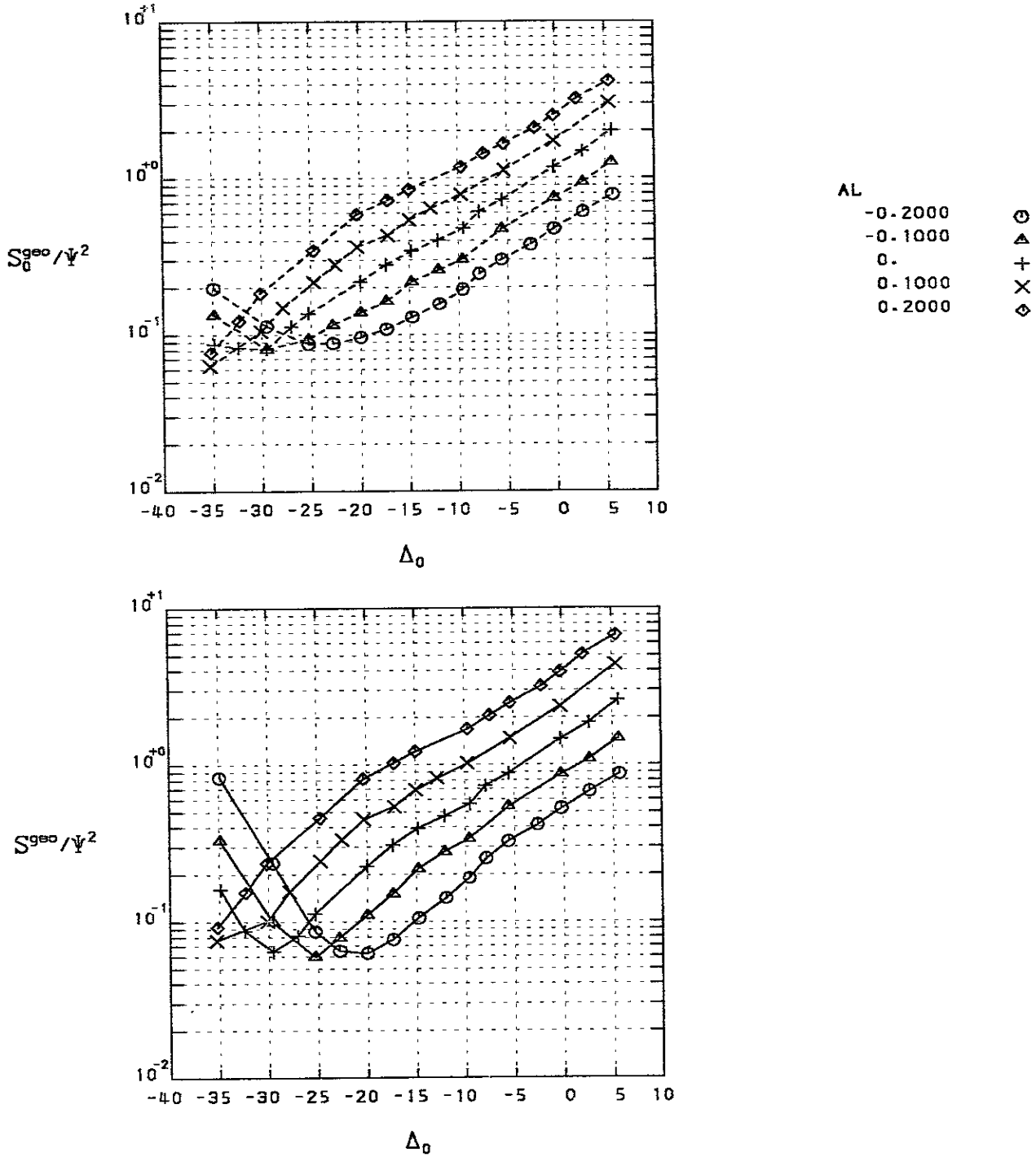
S_0^{geo}/Ψ^2
10^{+1}
10^{+0}
10^{-1}
10^{-2}
-40 -35 -30 -25 -20 -15 -10 -5 0 5 10
Δ_0
S^{geo}/Ψ^2
10^{+1}
10^{+0}
10^{-1}
10^{-2}
-40 -35 -30 -25 -20 -15 -10 -5 0 5 10
Δ_0
AL
-0.2000
-0.1000
0.
0.1000
0.2000

Fig.13

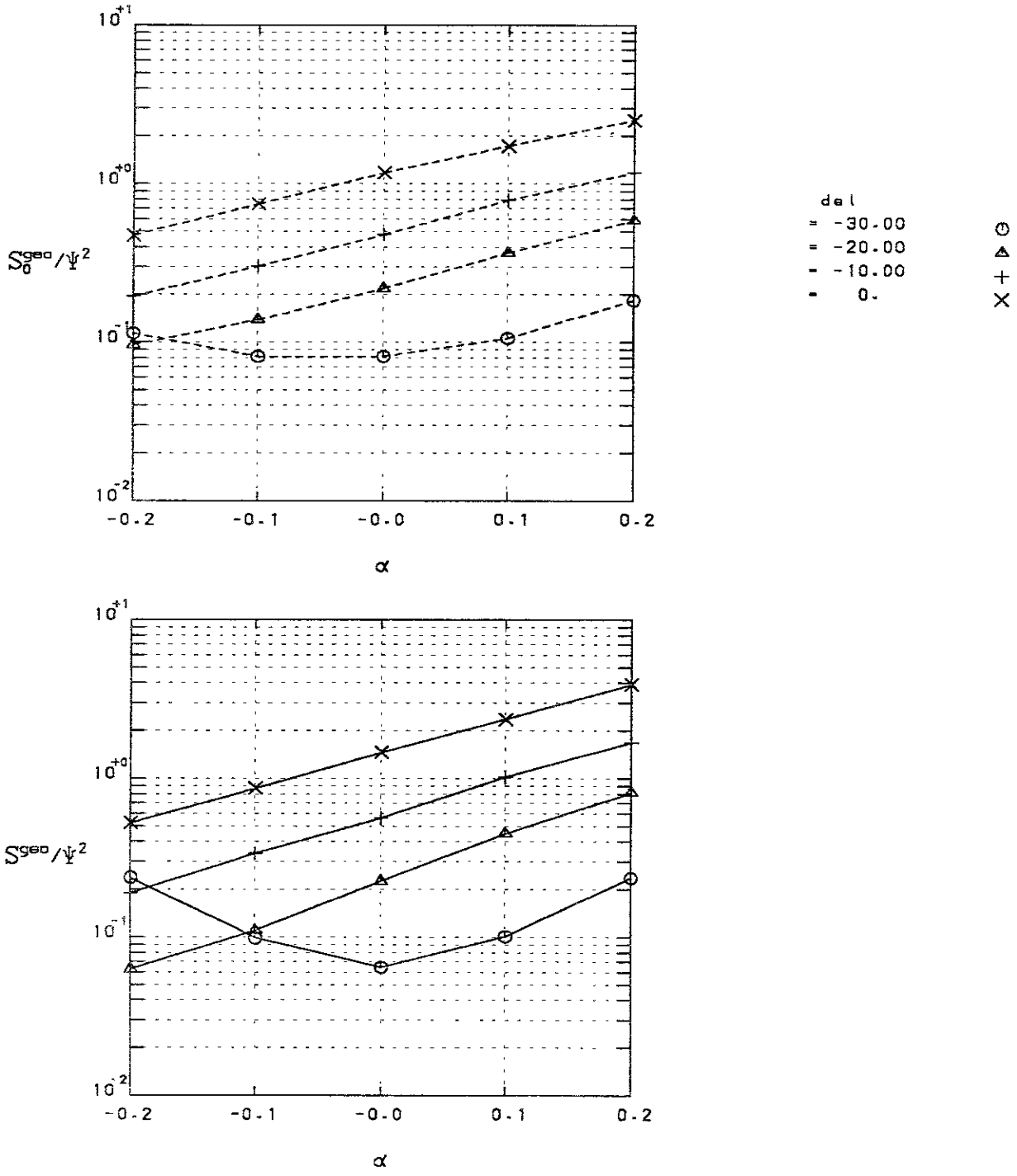
10^{+1}
10^{+0}
10^{-1}
10^{-2}
S_0^{geo}/Ψ^2
-0.2
-0.1
-0.0
0.1
0.2
α
del
= -30.00
= -20.00
= -10.00
= 0.
S^{geo}/Ψ^2

Fig.14

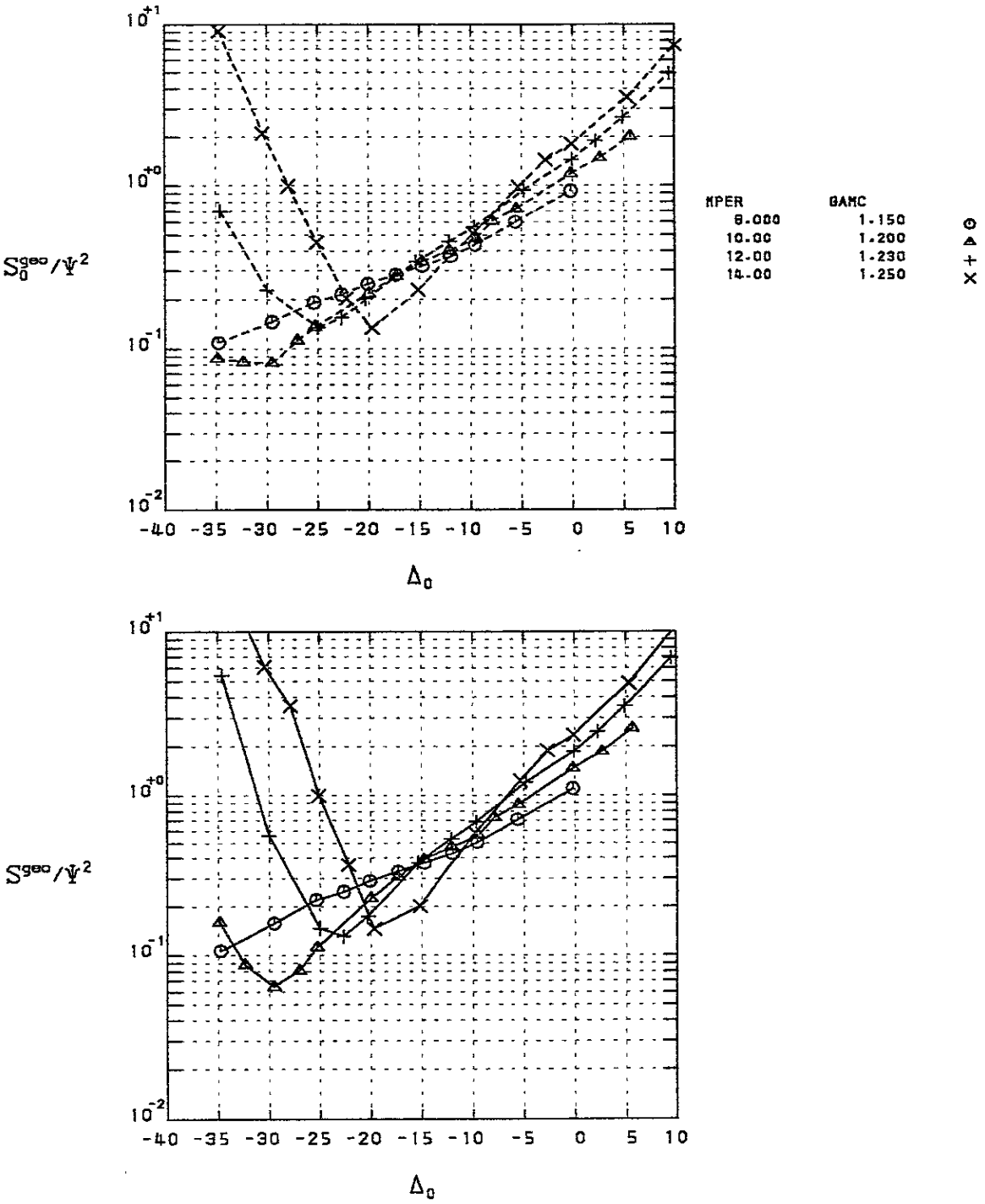
S_0^{geo}/Ψ^2
10^{+1}
10^{+0}
10^{-1}
10^{-2}
-40 -35 -30 -25 -20 -15 -10 -5 0 5 10
Δ_0
MPER GAMC
8.000 1.150
10.00 1.200
12.00 1.230
14.00 1.250
S^{geo}/Ψ^2
10^{+1}
10^{+0}
10^{-1}
10^{-2}
-40 -35 -30 -25 -20 -15 -10 -5 0 5 10
Δ_0

Fig.15